ACS APPLIED ENERGY MATERIALS

www.acsaem.org Article

Impacts of Solvent Washing on the Electrochemical Remediation of Commercial End-Of-Life Cathodes

Kae Fink,* Paul Gasper, Jaclyn E. Coyle, Nathaniel Sunderlin, and Shriram Santhanagopalan

Cite This: https://dx.doi.org/10.1021/acsaem.0c02260 Read Online

ACCESS | Metrics & More | Article Recommendations | Supporting Information

ABSTRACT: Changes to the surface structure and chemistry occurring throughout the functional lifetime of lithium-ion batteries (LIBs) may impact the effectiveness of end-of-life rejuvenation methods. Solvent washing prior to electrochemical relithiation is shown to both increase relithiation efficacy and beneficially alter the interfacial chemistry of the heavily degraded industrial cathode material. Four common solvents (acetone, diethyl carbonate, isopropyl alcohol, and propylene carbonate) are employed to investigate the role of varying physicochemical solvent properties on the mechanism of capacity recovery. Electrochemical (dQ/dV, EIS), structural (XRD), and chemical (SPME-GC-MS) analysis techniques are employed to comprehensively analyze solvent−cathode interactions. Highly nucleophilic solvents (acetone, DEC) are found to reduce cathode charge-transfer impedance and enable stable impedance growth throughout subsequent cycling. The use of nucleophilic solvents under mechanically aggressive washing conditions may also enable the reintroduction of bulk lattice oxygen, thereby restoring anionic redox capacity. Further, the four solvents are found to selectively remove a subset of surface species from the aged cathode material, including residual electrolyte, additives, and electrolyte−additive reaction products, which are qualitatively analyzed. Surface species removal by each solvent is correlated with the electrochemical performance of the correspondingly washed cathode, highlighting the importance of an optimized washing protocol for effective remediation in the context of direct LIB recycling. For the material under study, the use of a simple acetone-washing protocol prior to electrochemical relithiation enables up to 174% capacity recovery relative to unwashed/relithiated black mass.

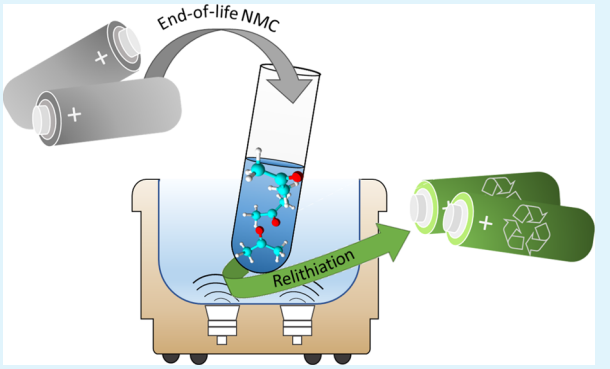

KEYWORDS: *direct recycling, solvent washing, electrochemical relithiation, cathode remediation, surface reconstruction, cathode−electrolyte interface*

1. INTRODUCTION

In the past decade, the number of electric vehicles on the road has increased dramatically. As of 2019, an estimated 7.2 million electric vehicles were in use globally, with electric vehicle sales accounting for a record 2.6% of all car sales.[1] By 2030, conservative projections predict a global EV stock of 140 million or ∼7% of the world's automotive fleet.[1] Central to the design of EVs is a mechanism for energy storage: a role that is increasingly being filled by Li-ion batteries (LIBs). Given LIBs' high charge-to-weight ratio, significant technical maturity, and rapidly decreasing production costs, LIBs are the predominant technology of choice for EVs and are predicted to remain so for at least another decade.[1] In fact, by 2030, transportation applications are predicted to account for 85% of the LIB production market.[2]

Along with the proliferation of LIBs in EVs will inevitably come the end-of-life of these units. The exponential increase in EVs will be mirrored by an exponential increase in spent LIBs—delayed by the lifetime of the battery (approximately 10 years).[3] It is estimated that, by 2030, the combined capacity of spent batteries from EVs will be comparable to current production volumes (∼100−120 GW h).[1] According to economic models, these LIBs should then be either refurbished or repurposed to maximize the product value and minimize life cycle impact.[4] However, these LIBs will eventually reach a true end-of-life and thus the development of effective LIB recycling protocols are crucial to maintain circularity of both economic value and resources.[4] The concept of direct recycling, or the recovery and rejuvenation of LIB components in maximally intact form, has gained traction in recent years.[5] Direct recycling of the cathode material is highly attractive from both a cost and resource perspective, as this approach retains the original engineered

Received: September 14, 2020
Accepted: November 17, 2020

https://dx.doi.org/10.1021/acsaem.0c02260
ACS Appl. Energy Mater. XXXX, XXX, XXX−XXX

value of the cathode while avoiding the use of energy-intensive smelters and environmentally problematic extractive solvents. To date, direct recycling methods have been demonstrated at the laboratory and pilot scales,[6,7] with a recent report by Sloop et al., suggesting the significant promise for the application of direct recycling methods to industrial LIB feedstocks.[7]

To achieve successful direct recycling, the cathode must be "rejuvenated" or returned to a condition enabling electrochemical performance equivalent to that of the pristine cathode material. Among the remediation techniques, relithiation—the reintroduction of Li into the cathode lattice to replenish the Li irreversibly lost to solid−electrolyte interface (SEI) formation and other side reactions—has perhaps garnered the greatest research focus. While mechanistic specifics vary, relithiation techniques generally aim to restore both the structure and stoichiometry of pristine cathode material through the re-intercalation of cyclable Li into the NMC matrix. Ideally, such techniques would render recycled materials indistinguishable from their virgin counterparts.

In relithiation studies to date, the material undergoing remediation treatment has largely been degraded under idealized conditions. There are relatively few studies reporting the relithiation of commercial cells that were recovered after "real world" use scenarios.[7] Notably, the electrolyte employed in the preparation of aged samples at the laboratory scale typically consists of Li salt in a standard blend of organic carbonates. While such an approach greatly simplifies the system of study, it does not accurately reflect the chemistry of commercial Li-ion cells, which regularly contain dozens of additives to enhance the performance or address specific electrolyte deficiencies.

With a growing focus on the rejuvenation of the spent cathode material, there has been relatively little emphasis on addressing the changes to cathode surface chemistry known to occur during a cell's lifetime and how this may impact subsequent capacity recovery. In particular, across numerous cathode chemistries, the growth of a resistive surface layer, analogous to the anode's solid electrolyte interface (SEI), has been reported.[8] This cathode−electrolyte interface (CEI) has been identified as the source of cathode interfacial resistance, which is the dominant contributor to cell impedance rise during both the cycling[8] and calendar-aging[9] of high-power Li-ion cells. Conclusive identification of CEI species is challenging because of the chemical complexity and irregularity of degradation products; however, numerous reports have identified common functional groups appearing in the CEI. These include Li_2CO_3,[10] hydrocarbons (C−C and C−H moieties),[11] polycarbonate-type compounds,[11,12] P═O moieties,[12] C═O moieties,[13] C−O−C moieties,[13] $ROCO_2Li$,[12,13] $(CH_2OCO_2Li)_2$,[13] Li_2O_2,[13] and LiF.[10,11] The additives in the commercial electrolyte and their associated degradation products compound this already-complex blend of surface species. Renfrew et al. have tested the reactivity of $LiNi_{0.6}Mn_{0.2}Co_{0.2}O_2$ with several electrolyte chemistries and two common additives (fluoroethylene carbonate and vinylene carbonate) and have reported the formation of a peroxo-like surface layer, particularly at higher voltages.[14] The effect of other commercial additives, and their associated degradation and reaction products, on the chemistry of the cathode surface has not broadly been studied.

Given the adverse impact of the CEI on the cathode performance during the cell's lifetime, it is anticipated that the presence of CEI may also inhibit cathode remediation strategies. Thus, establishing an optimal protocol for the removal of resistive surface species from commercial end-of-life cathodes is crucial to downstream cathode rejuvenation. Because of the relative novelty of Li-ion battery recycling, it is perhaps unsurprising that few studies to date have examined the process of removing CEI species and the subsequent impact on cathode performance. Waldmann et al. note that most experimentalists include a rinse in typical electrolyte solvents as part of postprocessing during cell disassembly and postmortem analysis.[15] This is typically performed with a carbonate (electrolyte) solvent—most commonly diethyl carbonate (DEC), dimethyl carbonate (DMC), or ethyl methyl carbonate (EMC)[15]—and aims to remove residual crystallized $LiPF_6$ or nonvolatile solvents. Thus, solvent washing is typically approached as an intermediate step to remove products that may inhibit other analyses, rather than an analytical approach in itself.[16] Because of this, solvent-washing parameters are largely arbitrary, and in fact, most authors omit details regarding their washing procedure (time, temperature, solvent choice, volume of solvent).[15] Only a few known studies have specifically explored the effects of solvent washing procedures on the chemistry of end-of-life electrodes, and these reports have focused on the targeted removal of SEI components from the anode.[17,18] Notably, Fang et al. have recently reported the use of gradient polarity wash to achieve selective and sequential extraction of SEI and near-SEI components on Cu and Si anodes. The authors suggest that the removal of electrolyte species from the anode is polarity-controlled and that the targeted removal of electrolyte species can be achieved via gradient washing.[18] An analogous systematic study of solvent effects on the efficacy of CEI removal—and, importantly, the effects of cathode washing on subsequent rejuvenation and performance—is lacking.

As has been noted, existing reports of cathode rinsing involve solvents whose chemistry is consistent with the native electrolyte system, that is, to remove reactive residual $LiPF_6$ without otherwise altering the surface chemistry.[15] However, in the context of preprocessing for cathode recycling, such surface alteration may be desired, and thus, the scope of solvent choice should be expanded beyond typical electrolyte solvents. Fang et al.'s study suggests the importance of solvent polarity on the removal of anode surface species.[18] While solvent polarity is undoubtedly a crucial parameter to consider, Dutkiewicz has proposed a more complex model for solvent classification.[19] Based on correlations between dielectric (β) and empirical solvent polarity (E_T) parameters, Dutkiewicz suggests that solvents can be categorized into several classes; notably for this study, class 1 contains weakly dipolar non-hydrogen-bonding donors (including ethers and carboxylic esters), class 2 contains dipolar non-hydrogen-bonding donors (including ketones), and class 3 contains hydrogen-bonding donors (including alcohols).[19] Further, the chemical structure and associated reactivity of the solvent must be considered. Fingerle et al. have outlined the primary modes of molecular interaction with the cathode surface, including physisorption; chemisorption; dissociation; ion transfer; and charge transfer.[20] Residual electrolyte solvents and intact $LiPF_6$ are weakly physiosorbed on the cathode surface and thus may easily be removed via rinsing with an

https://dx.doi.org/10.1021/acsaem.0c02260
ACS Appl. Energy Mater. XXXX, XXX, XXX−XXX

electrolyte solvent. However, end-of-life degradation species—particularly the complex products derived from the reaction of electrolyte and additives—are anticipated to experience multiple modes molecular interaction with the cathode surface and thus may require more reactive solvents.

To this end, in the present work, we have chosen to study solvents across both polarity classes and anticipated reactivities, based on chemical structure. In particular, diethyl carbonate—a common solvent used for electrode rinsing—has been selected to represent class 1 compounds; acetone—a cheap and readily available solvent—is a highly reactive class 2 solvent with moderate β and $E_T(30)$ values;[19] propylene carbonate—an electrolyte solvent—is a class 2 solvent with high β and $E_T(30)$ values;[19] and isopropyl alcohol—another inexpensive and common solvent—represents class 3 compounds. Study of these four solvents is intended to direct the future optimization of solvent parameters for electrode washing applications.

Thus, we herein present a systematic study of the effects of solvent washing on the surface chemistry and interfacial structure of cathodes recovered from heavily aged commercial cells. We demonstrate a simple and cost-effective washing protocol for aged cathode black mass, which may be implemented as a preprocessing step to relithiation in a direct recycling process design. We employ four common solvents representing a range of polarity and chemical reactivity: acetone, diethyl carbonate, isopropyl alcohol, and propylene carbonate. Effects are characterized using electrochemical analysis (capacity, dQ/dV, EIS), structural analysis X-ray diffraction (XRD), and chemical analysis gas chromatography−mass spectrometry (GC−MS). Further, we utilize the established washing protocol in conjunction with a simulated rejuvenation technique (electrochemical relithiation) to assess the impact of washing on subsequent capacity recovery in a model recycling process. The combination of solvent washing and electrochemical relithiation is found to enable capacity improvements of up to 174% relative to unwashed samples.

2. EXPERIMENTAL METHODS

2.1. Electrode Preparation. All electrode material used in the present study was obtained from commercial 40 A h pouch cells containing 34 pairs of electrodes and 68 layers of separator. In-house characterization via inductively coupled plasma atomic absorption spectroscopy (ICP-AAS) has suggested an approximate transition-metal stoichiometry of $Ni_{0.41}Mn_{0.36}Co_{0.23}$ in the as-received cathode material, with 92% active material (4.5% conductive carbon, 3.5% binder); as-received anodes contained 93% graphite active material (7% binder). "Fresh" electrodes were stored under inert conditions for approximately 1 year and under atmospheric conditions for a subsequent 1 year. "Cycle-aged" electrodes were recovered from cells that were first cycled at room temperature (~25 °C) within a voltage window of 3.0−4.1 V (2C charging rate; 1C discharging rate) for 5600 cycles and then stored under argon for approximately 1 year and under atmospheric conditions for a subsequent one year.

Black mass was removed from "cycle-aged" cathodes using a razor blade. For aged-unwashed samples, the black mass was directly processed in slurry format [97% black mass, 3% polyvinylidene difluoride (PVDF) binder in *N*-methyl pyrrolidone (NMP) solvent] and recast onto a fresh Al current collector foil. For aged-washed samples, ~0.5 g of black mass was added to 25 mL of each of four solvents [acetone, diethyl carbonate (DEC), isopropyl alcohol (IPA), and propylene carbonate (PC)]. The suspensions were sonicated for 30 min, followed by centrifugation (1440 rpm; 22 °C; 10 min). Supernatants were decanted, and the remaining solvent was dried under atmospheric conditions for ~10 h. To achieve full solvent removal, samples were then dried at low temperature (60 °C) for 24 h. Aged-washed samples were then processed in slurry format (97% black mass, 3% PVDF binder in NMP solvent) and recast onto fresh Al current collector foils.

2.2. Cell Assembly and Electrochemical Cycling. *2.2.1. Full-Cell Preparation and Cycling.* Two-electrode (i.e., full cell) coin cells were prepared from fresh, aged-unwashed, and aged-washed cathodes, each paired with a fresh anode. Cell assembly was conducted at room temperature in a glovebox, following overnight electrode drying at 105 °C. In all full cells, 50 μL of Gen 2 electrolyte (1.2 M $LiPF_6$ in EC/EMC = 3:7 by weight) and Celgard separator were used.

Following 6 h of rest at room temperature, full cells were cycled between 4.2 and 2.8 V at 25 °C using a multichannel cycler (Maccor). A constant-current/constant-voltage (CC/CV) protocol was utilized, with a charge/discharge rate of C/20 (~0.15 mA) for two initial formation cycles and a charge/discharge rate of C/10 (~0.3 mA) for a subsequent 100 cycles.

Discharge capacity is typically reported on a per-gram basis, with grams of electrochemically active NMC as the basis of normalization. However, the heavily aged samples utilized in this analysis were believed to contain significant levels of degradation products. Thus, capacity normalization for washed samples is calculated in two ways in this report: (i) specific discharge capacity (mA h/g) is calculated assuming the same proportion of NMC (92%) as in the pristine material, adjusted by the proportion of black mass (97%) in the recast slurry; (ii) normalized discharge capacity is reported as the ratio of the specific discharge capacity for each cell [as calculated in (i)] to the average specific discharge capacity of the fresh samples at the beginning of life (first cycle post-formation).

2.2.2. Simulated Electrochemical Relithiation. To simulate an electrochemical relithiation process, half coin cells were prepared from fresh, aged-unwashed, and aged-washed cathodes, each paired with a Li foil. Cell assembly was conducted at room temperature in a glovebox following overnight cathode drying at 105 °C. In all half cells, 50 μL of Gen 2 electrolyte (1.2 M $LiPF_6$ in EC/EMC = 3:7 by weight) and Celgard separator were used.

Half cells were rested for 6 h at room temperature and were then cycled at 25 °C using a multichannel cycler (Maccor). Four cycles were conducted at a constant C/10 current (~3 mA) between 4.3 and 3.0 V, with a 2 min rest period after each charge and discharge.

Following relithiation, half cells were disassembled in a glovebox, and the cathode was nondestructively recovered. Relithiated full cells were then constructed using the relithiated cathodes and fresh anode, as described in (a) above. CC/CV cycling at C/10 was conducted as described in (a) above, with cycling paused after every 20 cycles for intermediary electrochemical analysis. Discharge capacity is reported as described in (a) above.

2.3. Electrochemical Impedance Spectroscopy. Electrochemical impedance spectroscopy (EIS) was conducted on relithiated full cells after every 20 cycles. Prior to EIS analysis, all cells were charged at C/20 to 4.0 V and were held at a constant 4.0 V for 6 h. Cells were then rested for a minimum of 2 h to ensure that steady-state potential was achieved. Electrochemical impedance data were collected using a VersaSTAT 4 Potentiostat/Galvanostat (Princeton Applied Research) from 0.1 MHz to 1 mHz, with data recorded at 10 points per decade using an AC magnitude of 20 mV. Impedance was normalized by cathode active mass.

EIS data were analyzed by complex nonlinear least-squares (CNLLS) fitting of an equivalent circuit model. Before fitting EIS data, a linear Kramers−Kronig (lin-KK) test was performed to ensure that each EIS measurement was sound. The lin-KK test was performed using the open source analysis tool impedance.py.[21,22] Residual errors from lin-KK tests for all cells are shown in Figure S1, displaying no systematic measurement error across the data set. Data points at frequencies lower than the low-frequency turning point, identified as the first minima in the imaginary component of cell impedance when searching from low-to-high frequencies, were

https://dx.doi.org/10.1021/acsaem.0c02260
ACS Appl. Energy Mater. XXXX, XXX, XXX−XXX

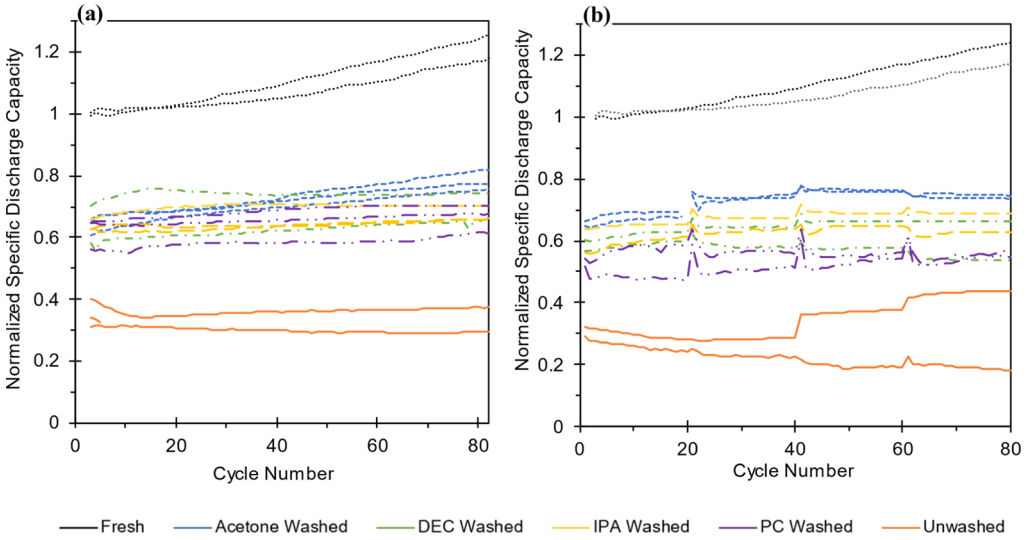

Figure 1. Electrochemical cycling performance of fresh and cycle-aged cathode material, with and without washing in various solvents: (a) washing condition only; (b) washing followed by electrochemical relithiation. In both cases, cycling data are shown for full cells (vs graphite anode) at C/10 CC/CV and two initial formation cycles (C/20 CC/CV) are omitted. Lines of the same color and linestyle represent replicate cells. Capacity is reported as a normalization by the average 3rd (1st post-formation) cycle specific discharge capacity (mA h/g) of the fresh sample replicates.

Table 1. Full-Cell Discharge Capacity of Cathodes under Washing Condition Only (Top) and Washing Followed by Subsequent Relithiation[a]

		cycle 10		cycle 50		cycle 80	
	sample	dischg. capacity (mA h/g)	% recovery (vs unwashed) (%)	dischg. capacity (mA h/g)	% recovery (vs unwashed) (%)	dischg. capacity (mA h/g)	% recovery (vs unwashed) (%)
washing condition only	U	33.61		33.46		34.16	
	Ac-W	68.32	103	75.05	124	79.85	134
	DEC-W	68.55	104	69.85	109	71.23	109
	IPA-W	66.09	97	67.68	102	68.70	101
	PC-W	63.25	88	65.95	97	67.71	98
washing plus relithiation	U-W-R	28.48		28.41		31.58	
	Ac-W-R	69.29	143	77.71	174	75.37	139
	DEC-W-R	61.59	116	63.09	122	61.03	93
	IPA-W-R	63.30	122	68.22	140	67.09	112
	PC-W-R	54.07	90	54.91	93	57.33	82

[a]Data are reported for cycles 10, 50, and 80 following formation. Capacity recovery for each washed sample is reported on a mA h/g-discharge basis as compared to the unwashed sample in that washing condition. All reported values reflect an average of cell replicates.

removed before fitting. Remaining data were then fit with an equivalent circuit model (ECM; Figure S2). To fit pseudo-semicircular features of the EIS data, three sets of parallel resistor-constant phase elements (ZARC elements) were used in series with a single resistor; this model has been shown to be accurate through both traditional impedance analysis and machine learning approaches.[23] Fits conducted with only two ZARC elements displayed systematic errors at high frequencies (Figure S2), and Nyquist and Bode phase plots of experimental data clearly displayed contributions from three distinct processes.

The ECM was fit to each data series using CNLLS via the SciPy function curve-fit, as implemented by impedance.py.[21] The shape factor of CPE elements was constrained between 0.8 and 1, ensuring that each ZARC element displayed relatively semicircular impedance.

2.4. X-ray Diffraction. Diffraction patterns of cast electrodes (composed of fresh, aged-unwashed, or aged-solvent-washed cathode) were obtained using a Rigaku Ultima IV diffractometer with CuKα radiation (40 kV, 40 mA) with a scintillation counter detector and 5 mm divergence slit. High-resolution scans were conducted from 10 to 90° 2θ (0.04° step size; 10 s dwell time). Reitveld refinement was conducted using Profex software.[24] Refinement details are discussed further in the text.

2.5. Gas Chromatography–Mass Spectrometry. To obtain a highly concentrated analyte suitable for chemical analysis, wash solutions were prepared using ~0.5 g of black mass in 5 mL of each of the four solvents analyzed (acetone, DEC, IPA, PC). The suspensions were sonicated for 30 min, followed by centrifugation (1440 rpm; 22 °C, 10 min). Supernatants were decanted and retained for analysis.

Direct-immersion solid-phase microextraction (SPME) sampling was employed to further concentrate the analyte. A polyacrylate (PA) SPME fiber (85 μm coating thickness) was exposed to 4 mL of each wash supernatant for 15 min under magnetic stirring (100 rpm). The PA fiber was desorbed in the injection port at 270 °C for 1.5 min. The fiber was rinsed with methanol (2 min, 100 rpm) and conditioned for 5 min (260 °C) between samples to avoid sample carryover.

Analysis was conducted using an Agilent 7890B gas chromatograph (GC) coupled with an Agilent 5977B mass spectrometer

https://dx.doi.org/10.1021/acsaem.0c02260
ACS Appl. Energy Mater. XXXX, XXX, XXX−XXX

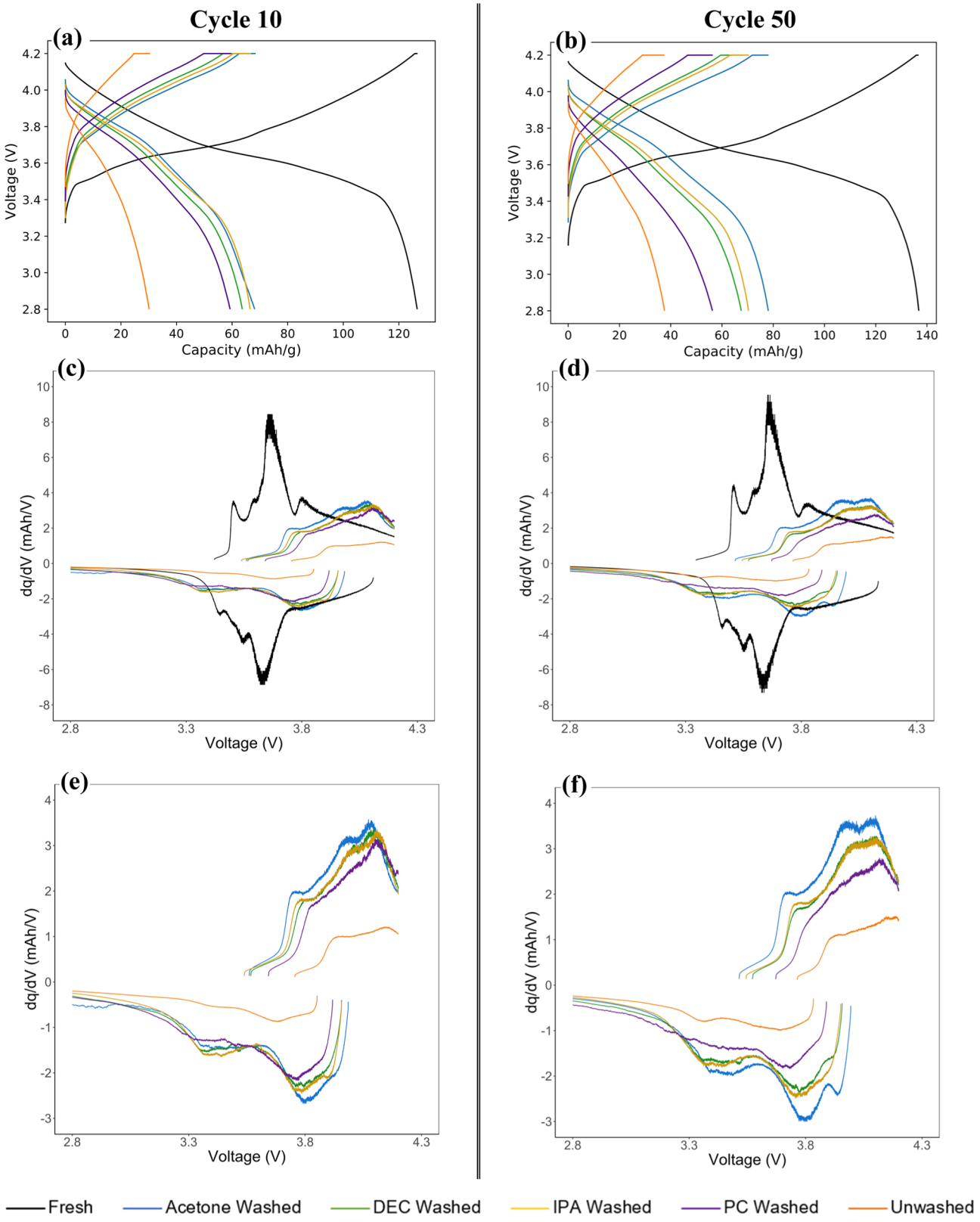

Figure 2. Discharge profiles (a,b) and corresponding differential capacity (dQ/dV) plots (c–f) for fresh and cycle-aged cathode material, with and without washing in various solvents, after 10 (a,c,e) and 50 (b,d,f) cycles following electrochemical relithiation. Plots (e,f) are insets of (c,d), respectively, with only cycle-aged samples shown to highlight distinctions between washing conditions.

(MS). A column optimized for the separation of electrolyte components (Wasson-ECE Instrumentation) was utilized. The system was run with He as carrier gas at a column flow of 1 mL/min in splitless mode, and the following column oven program, adapted from Horsthemke et al.:[25] a starting temperature of 40 °C was held for 2 min; the temperature was increased at a rate of 3 °C/min to 60 °C and then at 30 °C/min to 260 °C; and the final temperature of 260 °C was held for 2 min. MS was conducted using

https://dx.doi.org/10.1021/acsaem.0c02260
ACS Appl. Energy Mater. XXXX, XXX, XXX−XXX

electron ionization (EI) with an ion source temperature of 230 °C and a detector voltage of 1.02 kV in the range m/z = 10−300.

Spectra were analyzed using Enhanced ChemStation software (Agilent) and compounds were identified through MS spectral matching using the NIST MS Search Program v.2.3.

3. RESULTS AND DISCUSSION

3.1. Electrochemical Analysis. Electrochemical full-cell cycling data for fresh, aged-unwashed, and aged-solvent-washed cathodes are shown in Figure 1, and selected capacity values and statistics are tabulated in Table 1. As demonstrated in Figure 1a and Table 1, washing alone (without subsequent relithiation) is found to significantly increase discharge capacity. All washed samples show an 88% or greater capacity improvement (mA h/g) over unwashed samples under full-cell CC/CV cycling by cycle 10. Interestingly, the capacity is found to continuously increase for acetone-washed samples over 100 cycles, with these samples showing a 134% improvement over unwashed samples at cycle 80. This trend is also observed for fresh samples but does not appear to occur significantly for unwashed samples or samples subject to the other three washing conditions. By cycle 80, the performance of the aged cathode material is generally found to increase as unwashed (U) ≪ PC-washed (PC-W) < IPA-washed (IPA-W) < DEC-washed (DEC-W) < acetone-washed (Ac-W).

Figure 1b and Table 1 show the effect of washing, followed by electrochemical relithiation on full-cell discharge capacity. Cells were removed after each 20 cycles and charged to 4.0 V at a slower rate (C/20 followed by a trickle-charge voltage hold) for EIS analysis, resulting in a single-cycle elevated capacity value after formation and each subsequent 20 cycles. For all relithiated cells, capacity values were found to be slightly reduced on an absolute basis (mA h/g) as compared to their equivalent counterparts tested without relithiation. This is likely the result of the fabrication method, which involved cell disassembly from the half-cell (relithiation) condition and reassembly into a full cell. Electrode mass used for normalization was calculated prior to half-cell assembly and thus did not reflect any potential mass loss because of inadvertent mechanical damage during disassembly. However, the electrochemical performance of all relithiated cells is directly comparable, as methods were maintained consistently between samples.

By cycle 10, acetone-washed-relithiated (Ac-W-R) samples show a 143% capacity improvement over unwashed-relithiated (U-R) samples. Discharge capacity of Ac-W-R samples is again found to increase with full-cell cycling up to ∼60 cycles, with capacity reaching 174% of U-R samples by cycle 50. Capacity declines slightly on the subsequent cycles, with Ac-W-R sample capacity around 139% of U-R samples by cycle 80. Similar to the initial (nonrelithiated) condition, the performance is generally found to increase as U-R ≪ PC-washed-relithiated (PC-R) < IPA-washed-relithiated (IPA-W-R) ∼ DEC-washed-relithiated (DEC-W-R) < Ac-W-R.

Notably, the U-R cell replicates show significant variability in measured capacity, particularly after relithiation. This suggests heterogeneity in the degraded material, leading to variable efficacy of lithium reinsertion during relithiation. In contrast, all washed-relithiated samples show greater consistency between replicates than unwashed-relithiated samples, with Ac-W-R samples showing the tightest reproducibility. This behavior implies that solvent washing prior to relithiation may serve to homogenize material surface properties, enabling more uniform relithiation. The precise nature of these solvent−cathode interactions leading to the observed capacity performance will be taken up in more detail in the following sections.

Even for the best-performing Ac-W-R sample, electrochemical capacity is still greatly reduced (∼35%) relative to the fresh material. However, the contribution of solvent washing to both direct capacity recovery and the facilitation of subsequent electrochemical relithiation is remarkable. Additionally, the commercial cathode material used in this study was very heavily degraded, showing ∼70% capacity loss compared to the fresh material and demonstrating visible surface damage (pitting, deposits). This material represents a true worst-case for recycling, as electric vehicle batteries are typically considered to reach their end of life at 20−30% capacity loss (70−80% state-of-health).[26] Capacity recovery is anticipated to be significantly improved in less-degraded material.

The electrochemistry of the relithiated samples, with and without solvent washing, is further explored in Figure 2. Voltage profiles corresponding to cycles 10 and 50 following relithiation are shown in Figure 2a,b; a voltage profile for the fresh material is included for comparison. For consistency, the best-performing (i.e., highest discharge capacity) replicate for each condition is shown. At both cycle 10 and cycle 50, voltage plateaus are evident for the aged material, most notably for the Ac-W-R, DEC-W-R, and IPA-W-R samples. This profile shape indicates the presence of the spinel phase[27] and has previously been reported for this commercial material.[28] Structural analysis will be taken up in greater detail in the subsequent section.

Figure 2c−f presents the corresponding dQ/dV plots for cycles 10 and 50. The fresh material shows a dominant redox peak at ∼3.65 V, with smaller redox peaks at ∼3.5 V and ∼3.8 V. The dominant peak is attributed to $Co^{3+/4+}$ and $Ni^{2+/3+/4+}$ redox, which occurs at similar potentials and is thus typically indistinguishable in dQ/dV analysis.[29] The peak at ∼3.8 V is attributed to anionic redox,[29] and the peak at ∼3.5 V has been attributed to the minor activity of the reversible $Mn^{3+/4+}$ couple and additional anionic redox, which also typically overlap.[29,30] For the fresh material, minimal hysteresis is observed between charge and discharge.

For all aged samples, hysteresis is found to significantly increase relative to the fresh material, and voltage fade is observed for both charge and discharge profiles (Figure 2c,d). Gallagher et al. have proposed a physical model connecting these two phenomena, suggesting that the changes in the energy of Li-site occupancies lead to asymmetric transition-metal migration behavior upon discharge. Specifically, as voltage decreases, transition metals that have migrated into the tetrahedral sites of the Li layer may return to their original vacant octahedral site, which has shifted in energy (hysteresis), or may occupy another cubic site (voltage fade).[31] The loss of the dominant transition-metal redox peak in the aged material, in conjunction with both hysteresis and voltage fade, suggests significant transition-metal migration in this material, coupled with a structural rearrangement observed in both electrochemical and XRD measurements.

The reduction in electrochemical activity for the aged material can readily be explained via the above-described mechanism. More interesting, however, is the recovery in electrochemical redox for solvent-washed-relithiated material

https://dx.doi.org/10.1021/acsaem.0c02260
ACS Appl. Energy Mater. XXXX, XXX, XXX−XXX

Table 2. Characteristic Time Constants and the Physical Processes Attributed to Each Frequency Range of the Impedance Response from Graphitic Anodes, Intercalation Cathodes, and Full Cells of Lithium-Ion Batteries using Ethylene-Carbonate-Based Electrolytes Near Room Temperature at High States-Of-Charge[a]

	frequency range (Hz)	physical process	ref. #s
graphitic anodes	10^4	contact impedance (minor)	23,38,39
	10^3	interfacial charge transfer	
	10^1	interfacial charge transfer and ion/electron diffusion through porous electrodes	
intercalation cathodes	10^4 to 10^3	contact impedance	23,29,30,39
	10^1 to 10^0	interfacial charge transfer and ion/electron diffusion through porous electrodes	
full cells	10^4	contact impedance (anode and cathode; anode-dominated)	23,38,39
	10^4 to 10^3	contact impedance (anode and cathode; cathode-dominated); interfacial charge transfer (anode)	
	10^1 to 10^0	interfacial charge transfer; ion/electron diffusion through porous electrodes (anode and cathode)	

[a]Processes describing the diffusive/capacity tail at low frequencies have been omitted.

and the disparity observed between solvent conditions on electrochemical behavior. Previous work suggests that electrochemical relithiation alone restores aged cathodes to a structurally and electrochemically pristine state, by reinserting Li^+ into the NMC matrix to replenish depleted stores of cyclable Li^+.[32] If solvent washing were simply enabling more effective relithiation (i.e., by removal of resistive species preventing Li reinsertion), the electrochemical signature of rejuvenated materials would be expected to resemble pristine materials. However, Figure 2c,d demonstrates a drastic shift in the mechanism of electroactivity between fresh samples and relithiated samples in which capacity has been recovered. Nearly identical dQ/dV profiles between washed-relithiated and washed-only (without relithiation) samples (*not shown*) imply that the washing step itself, rather than the subsequent relithiation, is driving this behavior.

As shown in Figure 2e,f, the U-R sample shows virtually no electrochemical activity, with one minor redox peak at ~3.9 V/~3.7 V (charge/discharge). In contrast, each of the washed samples shows 2−3 redox peaks for both charge and discharge. It is probable that the central peaks for each of the washed samples (~4.0 V/~3.8 V charge/discharge) are attributable to Ni and Co redox, which has been recovered because of the removal of insulating surface species by solvent washing. These peaks show both significant voltage shift and hysteresis as compared to the fresh material, again attributable to asymmetric transition-metal migration.[31] The decrease in intensity of the dominant transition-metal redox peak has been previously observed for $LiNi_xCo_yMn_{(1-x-y)}$ (hereafter "NMC") materials following extended cycling, and the reduction in Ni/Co contribution to overall redox has been tied to incomplete cationic redox—particularly incomplete Ni-oxidation—in cycled materials.[30]

The growth in the redox peaks above and below the transition-metal peak for washed-relithiated materials implies a significant increase in bulk anionic redox and suggests that anionic redox may be dominating electrochemical activity in these refurbished cathodes. Anionic redox—the reversible electrochemical activity of bulk lattice oxygen (O^{2-}/O^{n-})—has only recently gained traction as a mechanistic framework for understanding the electrochemistry of NMC materials.[29,30,33] By this mechanism, Co and Ni are the main cationic redox couples,[29] with a gradual increase in $Mn^{3+/4+}$ activity also contributing to low-voltage redox after extended cycling.[30] At voltages above and below the Co/Ni (overlapping) dQ/dV peak, bulk anionic redox is found to contribute to charge compensation[29] and thus drive electrochemical activity.[29,30,33] Assat et al. have reported that reversible redox of bulk lattice oxygen may account for nearly half of observed capacity in NMC materials and remains active over extended cycling.[30] While the oxygen redox capacity has previously been found to decrease with cycling through the irreversible loss of lattice oxygen, either as O_2 or through the formation of degradation products,[30] the present analysis suggests that this anionic redox may be recoverable, and perhaps even enhanced, through solvent washing.

It has been suggested that solvent washing with polar solvents (alcohol,[14,34] water[14]) as a post-synthetic step induces surface reconstruction by the removal of certain surface defects, including carbonates and hydroxides.[14,34] We hypothesize that reaction with the four solvents, particularly under mechanically aggressive washing conditions (i.e., sonication), may similarly reconstruct the surface of the NMC particles. The strong nucleophilicity of acetone and the moderate nucleophilicity of DEC, PC, and IPA imply probable reduction at the NMC surface.[35,36] Specifically, a catalytic study on hydrotalcite-derived oxides (MnAlO, CoAlO, NiAlO, FeAlO) has suggested a mechanism whereby acetone adsorbs to weak acid sites on transition-metal oxide surfaces and is subsequently oxidized by reactive surface (lattice) oxygen.[35] This process is accelerated by the presence of oxygen vacancies in the lattice,[35] which is anticipated in our end-of-life cathode material. It is feasible that reduction by acetone—most strongly—or carbonates/alcohols—more weakly—could reintroduce oxygen back into the bulk lattice. This oxygen may be derived from either the solvent itself or adsorbed electrolyte/degradation products. Such a transformation of adsorbed oxygen species at the surface of p-type transition-metal oxides to lattice oxygen is thermodynamically favorable and has been proposed to proceed as O^{2-}(adsorbed) → O^{-}(adsorbed) → O^{2-}(lattice).[37] For the Ac-W-R sample in particular, the increase in anionic redox between cycles 10−50—observed as the growth of the dQ/dV discharge peak ~4.0V—provides evidence for lattice oxygen reintroduction, and this mechanism may be driving the observed increase in capacity during full-cell cycling. Structural studies provide additional evidence for this hypothesis, as will be discussed in the subsequent section.

EIS was performed after each 20 cycles for all relithiated full-cell samples to track impedance growth during cycling. Solvent washing is anticipated to reduce both contact resistance and interfacial charge-transfer resistance because of the removal of resistive degradation species, while relithiation is expected to impact the bulk structure of the cathode material, impacting ionic diffusion through the

https://dx.doi.org/10.1021/acsaem.0c02260
ACS Appl. Energy Mater. XXXX, XXX, XXX−XXX

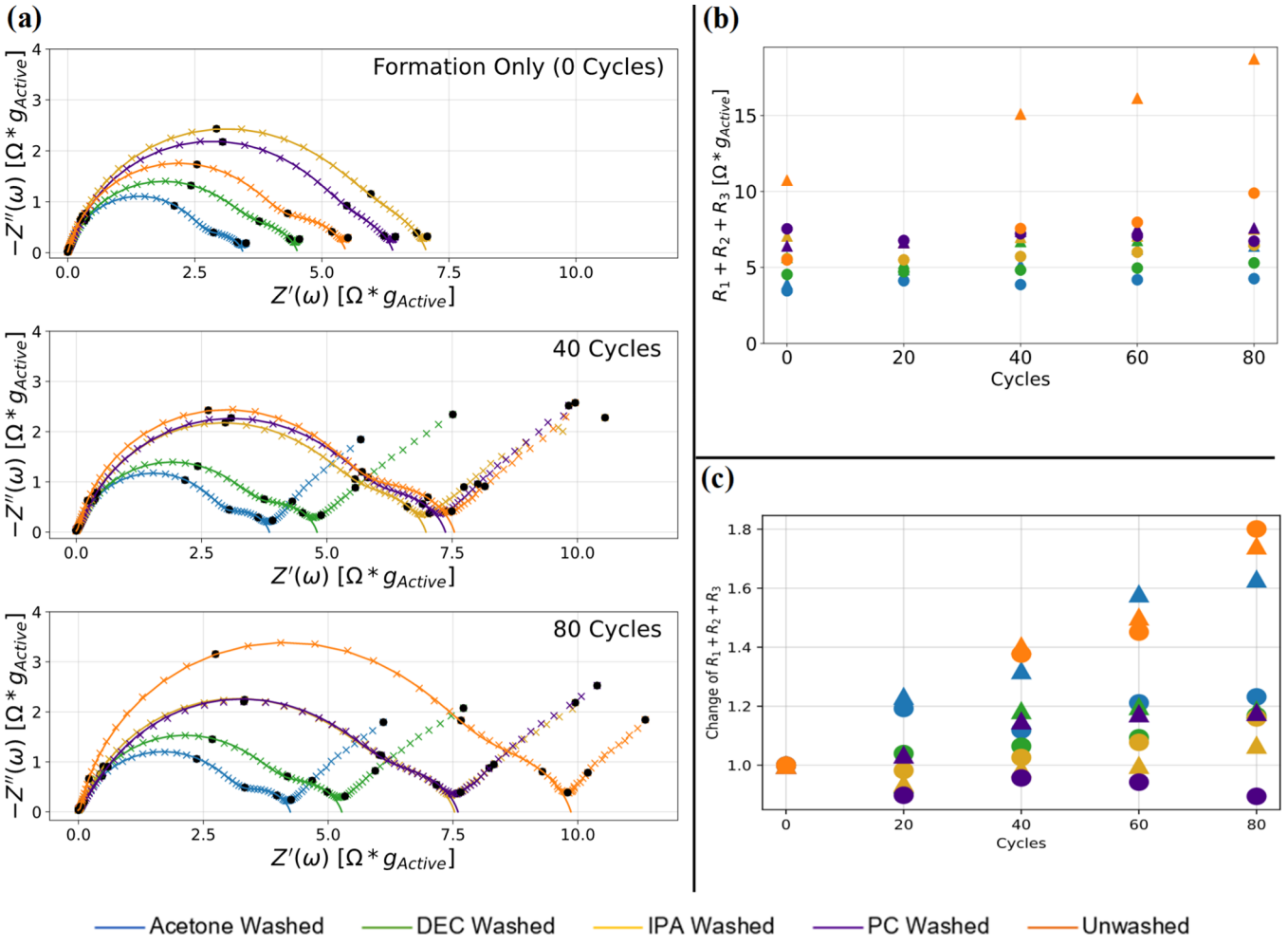

Figure 3. (a) Nyquist plots for one replicate of each condition (unwashed-relithiated or washed-relithiated) after formation (0 cycles; top); 40 cycles (middle); and 80 cycles (bottom) post-relithiation. Ohmic contributions are subtracted to aid comparison of the polarization impedance between cells. "X" indicates experimental data; solid line indicates ECM fit; black markers denote each frequency decade, starting at 10^5 Hz; (b) sum of deconvoluted resistances (R_1 + R_2 + R_3) for all relithiated cells after each 20 cycles; (c) change in the sum of the deconvoluted resistances for each cell, calculated via normalization by the initial value of impedance for each cell replicate. For (b,c), sample replicates for each washing condition are indicated using circular and triangular markers of the indicated color.

porous electrode as well as charge storage processes. These processes occur around different characteristic frequencies and are thus separable by deconvolution of the impedance spectra.

Equivalent circuit modeling was used to deconvolute the impedance response within the semicircular regime of the EIS measurements into three process, each modeling a distinct range of the frequency spectrum: high (10^5 Hz), middle (10^2 to 10^4 Hz), and low (10^0 to 10^1). An example of the separated contributions from each process to the overall impedance is shown in Figure S2. Residual errors from all fits show sinusoidal errors at frequencies from 10^0 to 10^3 Hz (Figure S3), suggesting that the equivalent circuit model may not be fully describing the features of the EIS spectra. However, error in this region does not impact the present analysis. More detailed studies have used transmission line models to model impedance behavior in this frequency range,[38] but such analysis is beyond the scope of this work.

In this study, only the contribution of the cathode to overall impedance is of interest. While the separate contributions from the anode and the cathode cannot be rigorously distinguished here, the impedance of each ZARC can be loosely attributed to physical processes using detailed studies of similar cells. The characteristic behaviors of the impedance response from each electrode and overall cell impedance are reported in Table 2. High frequencies (>10^3 Hz) are dominated by contact resistances (i.e., resistance to conduction of charged species on surfaces and across interfaces) and lower frequencies are dominated by interfacial charge-transfer processes and charged species transport through porous electrodes. While both electrodes contribute significant impedance across the entire frequency range, cell impedance is typically reported to be dominated by cathodic contributions.[23,39] Further, because all cells analyzed use identical anodes, differences between cells may reasonably be attributed to the disparate cathode washing treatments.

EIS spectra for unwashed-relithiated and washed-relithiated samples with Ohmic contributions subtracted are shown after formation, 40 cycles, and 80 cycles (Figure 3a). Consistent with discharge capacity performance, the impedance response from Ac-W-R and DEC-W-R samples is substantially lower than that of the IPA-W-R, PC-W-R, and U-R samples. IPA-W-R samples show slightly lower impedance than PC-W-R samples. Notably, the use of any solvent treatment before

https://dx.doi.org/10.1021/acsaem.0c02260
ACS Appl. Energy Mater. XXXX, XXX, XXX−XXX

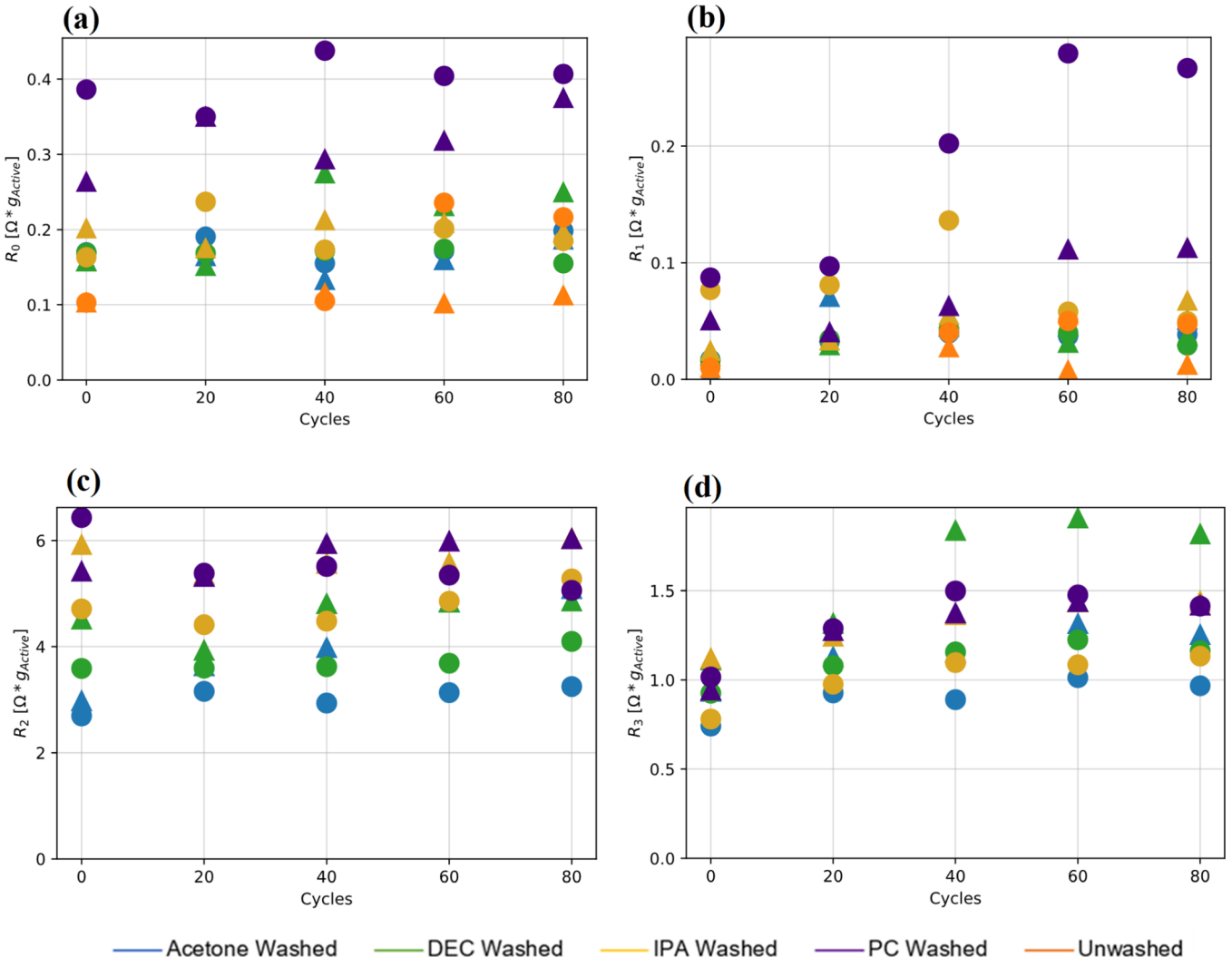

Figure 4. Deconvolutions of contributions to cell impedance: Ohmic resistance and three ZARC elements, tracked during electrochemical cycling of relithiated cells. (a) R_0: Ohmic resistance; (b) R_1: high-frequency (>10^4 Hz) contact resistance; (c) R_2: the dominant contribution to impedance near 10^3 Hz, primarily attributable to cathodic contact resistance; (d) R_3: the dominant contribution to impedance near 10^1 Hz, attributable to interfacial charge transfer and diffusion of charged species through the porous electrodes. For (c,d), data from U-R samples have been omitted for clarity of distinction between washing conditions (plots including U-R samples are shown in Figure S4).

relithiation appears to stabilize the cathode material, both in terms of overall polarization impedance (Figure 3b) and impedance stability with subsequent cycling (Figure 3c). This highlights the importance of solvent washing as a remediation procedure during direct recycling of end-of-life cathode materials. Of the washed and relithiated samples, Ac-W-R and PC-W-R samples show the most variability between replicates. Additionally, one Ac-W-R cell experienced substantial impedance growth during cycling, unique among all washed-relithiated cells. However, the impedance of this cell was still lower than those of the IPA-W-R and PC-W-R cells after 80 cycles.

The evolution of the ZARC elements R_0, R_1, R_2, and R_3 during cycling for each of the washed-relithiated samples is shown in Figure 4a–d, respectively. The Ohmic resistance (R_0; Figure 4a) is not expected to be influenced by washing, and this is observed for most cells. However, PC-W-R samples display significantly higher Ohmic resistance than any other cells. This suggests that the PC wash may leave a residue on the cathode surface, increasing the electronic resistance. This is verified by analysis of the high-frequency (>10^4 Hz) contact resistance (R_1; Figure 4b). PC-W-R cells—and, to some extent, IPA-W-R cells—display much larger R_1 values than all other samples, including unwashed samples, and these R_1 values continue to grow during cycling of the PC-W-R cells. In fact, one of the unwashed cells is found to have a lower impedance than either the IPA-W-R or PC-W-R samples (Figure 3b). Thus, while PC and IPA washing is beneficial for the overall stability of cell impedance, these solvents may also have deleterious impacts on the cathode materials.

Cell polarization is found to be dominated by the contributions of ZARC elements R_2 and R_3 (96.5% of the overall cell polarization resistance). R_2 dominates the impedance response near 10^3 Hz and is attributed to contact resistance. While washing does not necessarily reduce the contact impedance of the cathode materials, all washes improve the stability of contact resistance during cycling. This can be observed in the relatively stable R_2 during cycling of washed cells. Acetone and DEC are the most effective among the studied solvents in terms of reducing contact resistance compared to the unwashed case. The contact

https://dx.doi.org/10.1021/acsaem.0c02260
ACS Appl. Energy Mater. XXXX, XXX, XXX−XXX

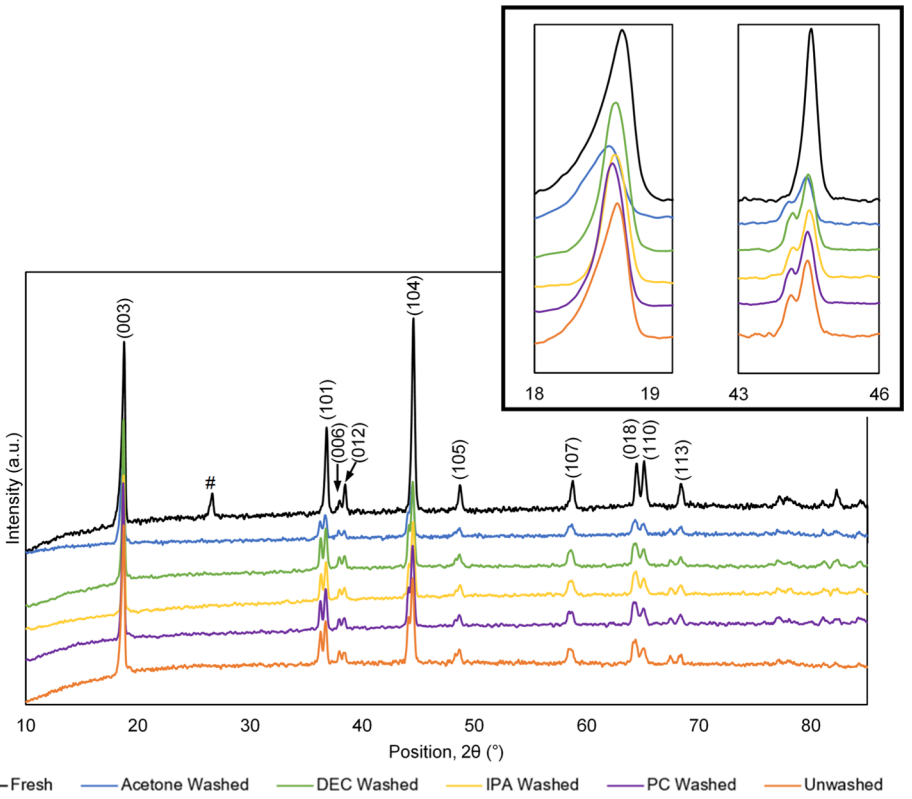

Figure 5. X-ray diffraction patterns of fresh and cycle-aged cathodes (cast electrodes), with and without solvent washing. Peak assignments are for trigonal (*R*3*m* space group) phase; # symbol indicates peak attributed to graphitic carbon.[40] Inset shows detail for (003) and (103) peaks.

Table 3. Lattice Parameters and Phase Distributions for Pristine, Aged-Unwashed, and Aged-Washed Samples[a]

sample	*a* (Å)	*c* (Å)	α-$NaFeO_2$ (*R*3*m*) (% ± ESD)	% Co_3O_4 (*Fd*3*m*) (% ± ESD)	NiO (*Fm*3*m*)(% ± ESD)
fresh	2.866(4)	14.23(9)	96.96 ± 0.70	2.38 ± 0.57	0.66 ± 0.46
unwashed	2.871(6)	14.27(6)	93.60 ± 1.30	4.10 ± 1.10	2.28 ± 0.71
acetone washed	2.867(7)	14.25(8)	92.50 ± 1.00	5.97 ± 0.87	1.54 ± 0.59
DEC washed	2.870(7)	14.27(1)	92.20 ± 1.30	7.30 ± 1.10	0.53 ± 0.75
IPA washed	2.869(1)	14.27(1)	90.60 ± 1.00	9.40 ± 1.00	0.0
PC washed	2.870(0)	14.27(0)	91.80 ± 1.10	8.20 ± 1.10	0.0

[a]Lattice parameters are reported for the trigonal (*R*3*m* space group) phase, with estimated standard deviation (ESD) < 0.004 Å for all samples. ESD for phase quantities is reported as a percentage. NMC reference pattern from Shinova et al.;[43] spinel (Co_3O_4) and rock salt (NiO) reference patterns from Profex structure database.[24]

resistance of Ac-W-R and DEC-W-R samples is lower than that of U-R samples immediately following formation and remains consistently lower than both PC-W-R and IPA-W-R samples during cycling.

Washing with any solvent also reduces the impedance contribution of R_3 (Figure S4), which dominates the overall impedance near 10^1 Hz and is attributed to interfacial charge transfer and charged species diffusion through the porous electrodes. Unlike R_2 values, which remain stable for all washed samples during cycling, R_3 values exhibit a slight increase during the first 40 cycles. As the low-frequency R_3 contribution is associated with bulk properties, such as interfacial charge transfer and ionic diffusion processes, the observed increase in R_3 upon initial cycling of relithiated samples may suggest changes to the crystal structure or internal stoichiometry as the relithiated particles redistribute lithium. This further supports the notion that washing may impact the mechanism of relithiation, rather than just improving the efficiency of relithiation.

Generally, the coefficient of variance for R_3 is found to be much less than the coefficient of variance of R_2 (0.136 for R_3 after formation, *c.f.* 0.282 for R_2 after formation). This implies that variations in solvent treatment have the greatest effect on high-frequency (surface-dependent) properties, such as contact resistance. Ac-W-R and DEC-W-R samples show the greatest reduction in overall impedance compared to U-W samples, consistent with electrochemical cycling results. Between these two conditions, DEC-W-R samples show a higher overall impedance but exhibit improved impedance stability throughout subsequent cycling.

3.2. Structural Analysis. Structural effects of both aging and subsequent solvent washing were assessed via XRD. XRD patterns for fresh, unwashed, and solvent-washed samples, prior to relithiation, are shown in Figure 5; selected parameters from Rietveld refinement are given in Table 3. Refinement was conducted using layered (trigonal α-$NaFeO_2$-type *R*3*m*), spinel (cubic Co_3O_4-type *Fd*3*m*), and rock salt (cubic NiO-type *Fm*3*m*) phases. A representative XRD diffractogram is given in Figure S5. The pristine material

https://dx.doi.org/10.1021/acsaem.0c02260
ACS Appl. Energy Mater. XXXX, XXX, XXX−XXX

shows a strong layered composition, with clear peak splitting between (006)/(012) peaks and (018)/(110) peaks indicating hexagonal ordering. Rietveld refinement suggests a composition of 97% layered *R*3*m* structure, with ∼3% phase impurities. The peak at ∼26.8° has previously been reported in composite cathode electrodes and has been attributed to graphitic conductive carbon.[40] For the fresh material, the *a* and *c* lattice parameters obtained for the trigonal phase are consistent with previous reports.[41,42]

For all aged samples, peak splitting is observed in several dominant peaks [(101), (104), (105), (113)], implying phase transformation. In particular, refinement suggests the growth of cubic spinel and rock salt phases, at the expense of the trigonal layered phase. It has been suggested that the phase change behavior of NMC materials is more complex than for other lithium-oxides, such as $LiCoO_2$ (LCO).[42] LCO materials are known to form cubic spinel phases, such as Co_3O_4 and $LiCo_2O_4$, upon extended cycling.[44] In addition, NMC materials may also form rock salt phases because of Li^+ deficiency and transition-metal (Ni^{2+}) migration.[42,45,46] Rock salt phase is found to be dominant under oxidative high-voltage environments.[45,46] The formation of both spinel and rock salt phases is observed for the present material, consistent with previous reports on NMC materials[42,45,46] and isostructural layered oxides.[47]

Quantified refinement results suggest that phase composition may be slightly dependent on washing condition, implying that washing may play a role in structural rearrangement, as well as impacting surface/lattice chemistry. All washed samples show a lower percentage of layered phase than unwashed samples but vary in the relative percentages of spinel and rock salt phases. In particular, Ac-W, DEC-W, and PC-W samples all show ∼92−92.5% layered phase, with the percentage of spinel phase increasing (rock salt phase decreasing) as Ac-W < DEC-W < PC-W. Interestingly, this is in precise inverse proportion to the electrochemical capacity of these samples. The IPA-W sample shows the lowest percentage of layered phase (90%) and the highest percentage of spinel phase and has the next-to-lowest electrochemical performance among the wash conditions.

The association of increased electrochemical performance (washed samples) with a reduced percentage of layered structure (as compared to the unwashed sample) appears to run counter to previous reports. Both spinel and rock salt phases are reported to lead to increased charge-transfer resistance, and thus decreased performance relative to the layered phase.[46] However, this apparently anomalous behavior may be explained by the emergence of an additional phase, manifest as the lower-angle split of the (101) peak and a lower-angle shoulder of the (104) peak. Rietveld refinement using the three phases commonly reported for degraded NMC materials (layered, spinel, rock salt) does not capture the emergence of these peaks. Notably, this phase is present for both unwashed and washed samples, implying that the material degradation, rather than the washing procedure, is responsible for the evolution of this additional phase. The nature of this phase will be further probed in future studies.

Analysis of *a* and *c* lattice parameters, shown in Table 3, provides additional information regarding the physical mechanism of structural change between fresh, unwashed, and washed samples. Specifically, an increase in *c* lattice parameter, corresponding to a shift of the (003) peak to lower angles, is observed for all aged samples, as compared to the fresh material. This is consistent with previous reports on cycled NMC material[41,42] and suggests increased electrostatic repulsion between MO_2 (M = Ni, Co, Mn) layers along the *c*-axis induced by lithium deficiency.[41,48] Nearly identical *c* lattice parameter values are observed for all aged cells, with the exception of the Ac-W sample, which shows a lower value. Ideally, in a remediated cathode, the (003) peak should shift back to a higher angle (lower *c* lattice parameter value);[42] this would indicate reduced oxygen repulsion, ostensibly because of restoring Li stores. However, the Ac-W sample analyzed had not yet been relithiated, further supporting the notion of reduction-induced structural rearrangement during the acetone-washing process.

Further, the *a* lattice parameter is anticipated to decrease following electrochemical cycling and resulting delithiation.[42,48] This has been attributed to the oxidation of Ni^{2+} to Ni^{3+} to achieve charge compensation in the delithiated state, leading to a contraction of the *a* plane because of the smaller ionic radius of Ni^{3+}.[48] In the present analysis, though, all aged samples show an *increase* in *a* lattice parameter relative to the fresh sample, with the *a* lattice parameter value increasing in relative inverse to electrochemical performance. This phenomenon may again be explained by changes to the lattice oxygen framework. In the aged cathode material under study, it is anticipated that lattice oxygen has been lost through conversion to electrolyte degradation species[14,20,30] and phase transformation. Charge compensation for the resulting oxygen vacancies may be achieved via the reduction of Ni^{3+} to Ni^{2+},[14] in direct opposition to the oxidation process anticipated in the delithiated state. It is probable that both processes are occurring simultaneously, with the reductive pathway apparently outweighing the oxidative one. It is possible that the reintroduction of lattice oxygen via solvent washing induces some oxidation of Ni^{2+} back to Ni^{3+}, resulting in a lower *a* lattice parameter for washed, versus unwashed, samples.

Taken together, the observed trends in lattice parameter values could also suggest the presence of positively charged electrolyte/additive degradation products within the Li layer, which are removed to various extents by the four solvent washing conditions. These products may both sterically and electrostatically increase repulsion between the oxygen layers (*c* lattice expansion), while causing transition-metal reduction to achieve charge compensation (*a* lattice expansion). The acetone-washing condition is found to restore these lattice parameters to values closest to that of the fresh material, corresponding with the greatest improvement in electrochemical capacity. Future studies will attempt to deconvolute these proposed mechanisms.

3.3. Chemical Analysis. In addition to changes to the bulk lattice oxygen network, it is anticipated that solvent washing will alter the surface chemistry of end-of-life cathodes by removing electrolyte degradation species, residual electrolyte additives, and reaction products evolving from both electrolyte and additives during the functional lifetime of the battery (i.e., CEI components). In addition to reducing surface resistance, this CEI removal would enable more effective relithiation by removing physical barriers to lithium intercalation. Thus, the four solvents have been assessed for their differential capabilities to dissolve CEI components present on the aged material under study. The species liberated by each solvent were assessed through the preparation of highly concentrated wash solutions, which

https://dx.doi.org/10.1021/acsaem.0c02260
ACS Appl. Energy Mater. XXXX, XXX, XXX−XXX

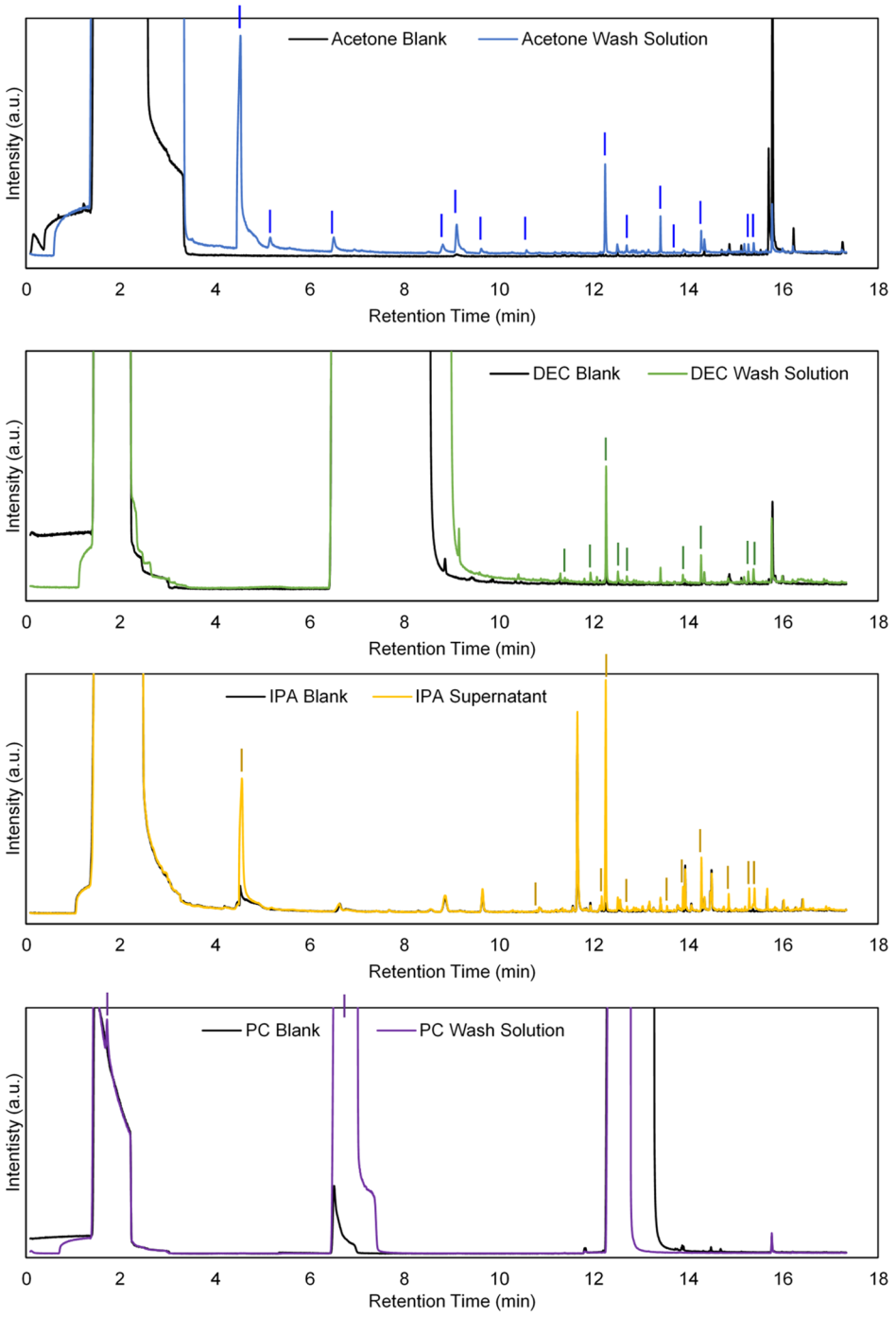

Figure 6. SPME GC−MS spectra of wash solutions for each of the four analyzed solvents, along with a corresponding solvent blank. Chemical species removed from the aged NMC (i.e., only appearing in the wash solution or appearing with significantly elevated intensity in the wash solution) are indicated with vertical lines and are listed in Table 4.

were then further concentrated using solid-phase microextraction (SPME).

Several previous studies have utilized GC-based methods to assess the chemical composition of end-of-life degradation products occurring in the liquid-phase electrolyte[25,49,50] or the gas phase following cycling and/or cell abuse.[49−51] However, this is the first known report investigating the selectivity of various solvents for electrolyte and CEI components on commercially relevant NMC cathode materials. GC−MS spectra for each of the wash solutions are shown in Figure 6, along with a corresponding blank for each solvent. Comparison with a solvent blank is crucial to eliminate background signals evolved from both solvent impurities and inherent SPME fiber signals, as well as any species that may evolve from fiber−solvent interactions. Species unique to the wash solution (i.e., not present in the blank) are indicated with vertical bars and a compiled tabulation of all species removed, above the instrument detection limit, is found in Table 4. Table 4 also includes an assignment of the presumed origin of each chemical species.[52]

The species removed by solvent washing may be grouped into three broad categories: electrolyte degradation products,

https://dx.doi.org/10.1021/acsaem.0c02260
ACS Appl. Energy Mater. XXXX, XXX, XXX−XXX

Table 4. Chemical Compounds Removed from End-Of-Life NMC via Sonication in Each of Four Solvents, Arranged with Increasing Retention Time[a]

#	Compound	Source	RT (min)	Acetone	DEC	IPA	PC
1	Diisopropyl carbonate	Elec. Deg.	1.71	X	X	X	✓
2	Ethylene glycol	Elec. Deg.	4.53	✓	X	✓	X
3	1-[(4-bromo-2,5-dimethoxyphenyl)methyl]-piperazine	Elec.-Add. Reac,	5.15	✓	X	X	X
4	Diethyl carbonate	Elec. Deg.	6.60	✓	---	X	✓
5	5-(1-methylethylidene)-1,3-cyclopentadiene	Elec.-Add. Reac,	8.80	✓	---	X	X
6	Diacetone alcohol	Solvent Reac.	9.10	✓	---	X	X
7	Bicyclo[2.1.1]hex-2-ene, 2-ethenyl	Elec.-Add. Reac,	9.62	✓	X	X	X
8	Cyclohexanone	Elec.-Add. Reac,	10.57	✓	X	X	X
9	2,3-heptadien-5-yne, 2,4-dimethyl	Elec. Deg.	10.84	X	X	✓	X
10	2,5,6-trimethyl decane	Elec. Deg.	11.38	X	✓	X	X
11	Hydrazine-carboxylic acid, ethyl ester	Elec.-Add. Reac,	11.93	X	✓	X	X
12	Propyl nitrite	Additive Deg.	12.16	X	X	✓	X
13	Ethylene carbonate	Elec. Deg.	12.23	✓	✓	✓	X
14	Diethyl butyl phosphate or diethyl pentyl phosphate	Elec. Deg.	12.69	✓	✓	✓	X
15	1-hexadecanol or 1-tetradecene	Elec.-Add. Reac,	13.40	✓	★	✓	X
16	Diethyl 2,5-Dioxahexanedioate	Elec. Deg.	13.88	✓	✓	✓	X
17	Biphenyl	Additive	14.26	✓	✓	✓	X
18	Ethyl 4-ethoxybenzoate	Elec.-Add. Reac.	14.85	✓	✓	✓	X
19	Diethyl phthalate	Elec.-Add. Reac,	15.17	✓	✓	✓	X
20	Diethyl terephthalate	Elec.-Add. Reac,	15.26	✓	✓	✓	X

[a]Check mark (green shading) indicates that the given compound was detected in the wash solution of the given solvent; dashed line (orange shading) indicates no detection of the given compound in the wash solution of the given solvent but potential confounding because of coelution with another chemical species; "X" (red shading) indicates no detection of the given compound, with no potential confounding. Star symbol (★, green shading) indicates a species that was observed in both blank and wash solution.

additives, and electrolyte−additive reaction products. Electrolyte degradation products are primarily carbonate derivatives and are the typically reported components of the CEI.[10−14] Two notable studies have developed a physical model for the evolution of carbonate degradation products on LCO,[20,53] which is presumed to progress similarly on NMC. This process includes initial adsorption of carbonate solvent onto the oxide surface, followed by a nucleophilic reaction of surface oxygen with the carbonate's carbonyl carbon.[53] Deintercalated Li ions transfer to the surface and are dissolved in the carbonate adsorbate phase, leading to the formation of lithiated reaction products.[20,53] The authors of these two studies reported similar mechanisms for both ethylene carbonate and diethyl carbonate electrolytes, and in fact, a more recent report studying the reactions of NMC-622 with several electrolyte mixtures concluded that the reactivity was remarkably similar across NMC materials and all carbonate electrolytes.[14] In particular, nucleophilic attack by oxygen (surface[14,20,53] and bulk lattice[14,53,54]) and migration and solvation of Li at the surface are believed to be the dominant mechanisms resulting in the formation of electrolyte degradation products.[14,20,30,53,54] Several of the components detected in the wash solution (Table 4) are known electrolyte components and may have been adsorbed on the surface [ethylene carbonate (EC; #11), diethyl carbonate (DEC; #4)]; others contain structural moieties (carbonate, hydrocarbon, P═O) suggesting electrolyte degradation products that may have been covalently bound to the NMC surface. These compounds include diisopropyl carbonate (#1); 2,4-dimethyl-2,3-heptadien-5-yne (#9); 2,5,6-trimethyl decane (#10); butyl diethyl phosphate/diethyl pentyl phosphate (indistinguishable in the present analysis; #14); and diethyl 2,5-dioxahexanedioate (#16). Ethylene glycol (EG; #2) is a reported hydrolysis product of EC, formed in conjunction with CO_2 in the presence of water.[55,56] The room-temperature hydrolysis of EC to EG is a thermodynamically slow process at room temperature,[55] but this reaction may be anticipated for the present cathode material, given the long storage period under atmospheric conditions. Additionally, it is plausible that EG may have evolved through the solvent washing process itself, as basic moieties have been shown to catalyze EC ring opening, leading to EG and poly-EG formation at room temperature.[55,57]

In commercial cells, additives are typically included to address specific deficiencies in the standard carbonate solution or to provide performance enhancement or safety protection under specific operating conditions. It is probable that the commercial cell from which the present cathode material was harvested contained several to dozens of additives, and the chemistry of the species recovered from the wash solutions supports this notion. Propyl nitrite (#12) is the probable reduced product of propyl nitrate, an additive used for SEI formation.[58] Biphenyl (#17) is an additive intended to form the CEI[59] or form the SEI in cases of overcharge (a so-called "shutdown molecule").[60−62]

Finally, several of the compounds recovered from the wash solutions appear to be reaction products between additives and electrolyte components, based on their chemical composition. The combination of Li and F species in the electrolyte and transition-metal species such as Co, which is frequently used in catalysis, serves as a highly reactive environment for the evolution of complex chemical species. In the present analysis, we have identified seven such species.

https://dx.doi.org/10.1021/acsaem.0c02260
ACS Appl. Energy Mater. XXXX, XXX, XXX−XXX

While we have attempted to identify these species based on mass fragment reconstruction, NIST database matching, and reaction chemistry rationale, it should be noted that such reaction products tend to be structurally complex and often lack appropriate standards for identification. In Table 4, these reaction products have been identified according to the highest-percentage mass spectrum NIST match, with the recognition that precise stoichiometry and isomeric structure may vary slightly from these assignments. Thus, we aim to emphasize the reactive pathways capable of producing species with the observed mass fragment moieties, rather than the definitive identity of specific reaction products.

Piperazine, 1-[(4-bromo-2,5-dimethoxyphenyl)methyl]- (#3) is a Br-containing, bicyclic, aromatic compound that may have formed from the reaction of a Br-containing additive (e.g., 4-bromobenzyl isocyanate or 3-bromothiophene, both intended to polymerize at the cathode;[60,63] or α-bromo-γ-butyrolactone, intended to form the SEI[64] or reduce corrosion[65]) with another aromatic additive. 1,3-Cyclopentadiene, 5-(1-methylethylidene)- (#5) may have evolved from cyclohexylbenzene, an additive used for overcharge protection that unstable in the presence of oxidizing agents.[61] Bicyclo[2.1.1]hex-2-ene, 2-ethenyl (#7) is a bicyclic alkene, perhaps evolved from aromatic additives such as cyclohexylbenzene. Cyclohexanone (#8) was likely evolved from the oxidation of cyclohexane in air, which typically proceeds in the presence of Co catalysts. Cyclohexane has been used to improve the first cycle efficiency by increasing the elasticity of the PVDF binder[66] and improving the wettability of the separator.[67] Hydrazine-carboxylic acid, ethyl ester (#11) could form from the reaction of carbonate species with amine-containing compounds. Amines are typically added to react with residual H_2O and thereby prevent HF formation (so-called HF scavengers).[68,69] Compound #15 is a long-chain hydrocarbon (mass spectra corresponding to either 1-hexadecanol or 1-tetradecene, with equal NIST matching confidence), suggesting an origin as an electrolyte degradation product but also contains alcohol or alkene moieties, implying further reaction, perhaps with additives. Ethyl 4-ethoxybenzoate (#18) contains carbonate and ester moieties—likely evolved from electrolyte—but also aromaticity, ostensibly from a benzene derivative additive such as biphenyl or cyclohexylbenzene. Diethyl phthalate (#19) and 1,4-diethyl terephthalate (#20) are both phthalate esters, which may also have evolved from the reaction of a carbonate degradation product and a benzene derivative. Finally, diacetone alcohol (#6) appears to be an aldol condensation product of acetone, implying that this species may have been formed via catalysis during the washing process, rather than being removed from the aged black mass.

With the exception of electrolyte solvent residues (DEC, EC) and possibly unreacted additives (ethylene glycol, biphenyl), which may have been adsorbed on the NMC surface, we anticipate that the species removed via solvent washing had been ionically or covalently bound within the NMC lattice. This would be consistent with their mechanism of their evolution, involving the covalent interactions with surface oxygen described for electrolyte degradation products and/or catalytic reactions with the transition metals. Thus, effective removal of these products may involve chemical reaction in addition to a pure solvation mechanism.

The adage "like-dissolves-like" offers an initial rationale for the nature of the products removed by each solvent. Acetone, a polar ketone, is found to dissolve polar, non-H-bonding compounds, but is less effective in solvating nonpolar compounds. Diethyl carbonate, a carbonate ester, effectively removes weakly polar, non-H-bonding compounds, but is unable to solvate more highly polar compounds. Isopropyl alcohol is an alkyl alcohol, and as such dissolves polar, H-bonding compounds, but is ineffective at dissolving nonpolar species. Finally, propylene carbonate is a cyclic carbonate ester, anticipated to dissolve polar, non-H-bonding compounds—similar to acetone. However, PC is found to be largely ineffective at removing any species whatsoever, under the present analysis conditions. This is somewhat surprising, as PC has previously been employed as a solvent for GC−MS analysis of electrolyte and electrolyte degradation products.[50] The lack of solvation activity may be explained by a significant increase in DEC between the blank and the wash solution, suggesting a potential reactive conversion from PC to DEC. Such a process has been reported for the synthesis of DEC in the presence of an alcohol and transition-metal catalysts, an environment quite similar to the present system.[70] PC is also expected to have greater steric hindrance because of its cyclic structure, as compared to the smaller molecular form of the other solvents.

In addition to polarity, structural reactivity must be considered in the assessment of the various solvents' efficacy in the context of CEI removal. The structure of each of the four solvents, which has briefly been discussed, may affect both the ability to induce surface transformation (i.e., reintroduction of lattice oxygen) and the removal of passivating or electrochemically interfering degradation species. As a ketone, acetone is the most strongly nucleophilic of the solvents in this study due to lone-pair electrons on the carbonyl carbon with no additional resonance-stabilizing moieties. This makes acetone broadly reactive to both electrolyte degradation products and a variety of organic additives. Carbonate esters, such as diethyl carbonate and propylene carbonate, are more weakly nucleophilic because of the stabilizing resonance of the ester oxygen. This may be beneficial in the removal of certain electrolyte degradation products but is unlikely to be effective across a broad and chemically diverse class of additives. Alcohols, such as isopropyl alcohol, are amphoteric, suggesting both nucleophilic and electrophilic reactivity; however, H-bonding properties cause high intramolecular interactions between solvent molecules, reducing reactivity.

Thus, the ability of each solvent to liberate various CEI species is suggested to depend on both solvent polarity and underlying structure, including sterics. Acetone is found to successfully remove all three classes of end-of-life compounds identified: electrolyte degradation products, additives, and electrolyte−additive reaction products. DEC is able to remove electrolyte degradation products and certain electrolyte−additive reaction products but is unable to remove polar additives—notably, ethylene glycol, an insulating hydrocarbon that appears at high intensities in acetone and IPA washes in this study. IPA removes polar additives and moderately polar or polarizable electrolyte degradation products but is ineffective at removing nonpolar electrolyte degradation products and several weakly polar or nonpolar electrolyte−additive reaction products. Finally, PC is found to be a relatively ineffectual solvent in the present analysis. This may be the result of steric hindrance and reactivity in the presence of alcohol-containing additives and transition-metal catalysts

https://dx.doi.org/10.1021/acsaem.0c02260
ACS Appl. Energy Mater. XXXX, XXX, XXX−XXX

to form DEC. However, given previous successful reports utilizing this solvent for end-of-life electrode analysis,[50] additional studies should be undertaken to verify the present results and rule out compatibility issues with the PA SPME fiber as a cause of the poor solvent performance.

While the specific impact of CEI removal on lithium reuptake is not quantified in the present report, there is a strong correlation between the number and breadth of components liberated and the electrochemical performance of the rejuvenated cells. In particular, acetone is found to most effectively remove a chemically diverse range of CEI components, and Ac-W-R samples show the highest capacity of the remediated samples; similar trends are observed for the other washing conditions. It is anticipated that the removal of surface- and pore-blocking species enables enhanced Li intercalation during electrochemical relithiation, thereby contributing to the observed increase in capacity. Quantification of Li stores following each solvent treatment will help to more clearly delineate the synergistic effects of direct solvent interactions (i.e., surface reconstruction) and CEI removal (enabling increased Li uptake) on NMC rejuvenation. Such work is the focus of ongoing studies.

4. CONCLUSIONS

Heavily degraded commercial cathode material, cycled and calendar aged to ∼30% state-of-health, has been significantly rejuvenated through a combination of solvent washing and electrochemical relithiation. In particular, sonication of spent black mass in acetone followed by relithiation enables capacity recovery of up to 174% relative to unwashed/relithiated black mass. The capacity is stable for remediated cathodes over at least 80 cycles post-relithiation. The present analysis implies a complex role of solvent washing in the performance of aged cathode materials and offers a promising path toward the integration of washing techniques in a broader cathode recycling protocol.

Electrochemical, structural, and chemical analysis of materials washed in four different solvents (acetone, diethyl carbonate, isopropyl alcohol, and propylene carbonate) suggest a multifold role of the organic solvent in the observed capacity performance. Differential capacity analysis implies a shift in the mechanism of electroactivity between fresh and aged samples, with capacity recovery for washed samples largely attributable to increased anionic redox, rather than recovery of transition-metal redox. This indicates that anionic redox may be recovered by solvent interactions. We propose that use of nucleophilic solvents, in conjunction with mechanically aggressive washing conditions (sonication), can reduce the NMC surface and allow for reintroduction of oxygen back into the bulk lattice.

Structural analysis provides further evidence for this mechanism. An increase in *c* lattice parameter is observed for aged materials as compared to the pristine material, consistent with transition metal−oxygen repulsion induced by delithiation. However, acetone-washed samples show a lower *c* parameter prior to relithiation, suggesting that bulk structural rearrangement may be achieved during the solvent washing process. Further, reduced *a* lattice parameter values for washed samples as compared to unwashed samples may be attributed to Ni-oxidation, ostensibly because of lattice oxygen reintroduction during solvent washing. Additionally, we hypothesize that positively charged electrolyte/additive degradation products may accumulate within the Li layer during cycling/aging, inducing steric and electrostatic repulsion between the oxygen layers (*c* lattice expansion) and transition-metal reduction (*a* lattice expansion). Selective removal of these degradation products may account for the observed lattice parameter shifts between washing conditions.

Finally, both impedance and chemical analysis suggest the role of surface chemistry on electrode performance. While any form of solvent washing is found to decrease overall impedance and reduce impedance growth during subsequent cycling, the nature of the solvent is found to most dramatically impact charge-transfer resistance. Specifically, acetone- and DEC-washed samples show reduced charge-transfer resistance, suggesting the removal of insulating surface species. Analysis of highly concentrated wash solutions reveals three categories of species removed from commercial black mass by solvent washing: electrolyte degradation products, additives, and electrolyte−additive reaction products. The solvent structure is found to impact selectivity for various species, and the removal of passivating surface species via washing is believed to contribute to the observed capacity recovery for washed samples. Acetone, a ketone with moderate polarity and the highest nucleophilicity of the solvents studied, appears to enable most effective removal of a broad scope of degradation products covalently bound within the NMC lattice.

The simple and cost-effective solvent-washing technique presented in this study, applied in conjunction with cathode rejuvenation techniques, is intended to inform direct recycling process design. However, significant work remains to optimize this solvent-washing protocol at scale. Analysis should be expanded to multiple commercial end-of-life materials to verify the breadth of these findings. Further, the solvent properties we have identified as impactful to capacity recovery (nucleophilicity, polarity, steric hindrance) should be applied to the tailored solvent design, and studies of solvent mixtures and gradient washing are warranted. Finally, in moving toward practical scale-up of a direct recycling process, techno-economic factors and safety considerations (e.g., solvent flammability) will be crucial to informing an optimal solvent choice.

■ ASSOCIATED CONTENT

Supporting Information

The Supporting Information is available free of charge at https://pubs.acs.org/doi/10.1021/acsaem.0c02260.

Lin-KK test residual errors; ECM fits; ECM residual errors; reproduction of Figure 4c,d, including unwashed samples; and representative refined XRD diffractogram (PDF)

■ AUTHOR INFORMATION

Corresponding Author

Kae Fink − *National Renewable Energy Laboratory, Golden, Colorado 80401, United States;* orcid.org/0000-0001-9363-4632; Email: Kae.Fink@nrel.gov

Authors

Paul Gasper − *National Renewable Energy Laboratory, Golden, Colorado 80401, United States;* orcid.org/0000-0001-8834-9458

https://dx.doi.org/10.1021/acsaem.0c02260
ACS Appl. Energy Mater. XXXX, XXX, XXX−XXX

Jaclyn E. Coyle − *National Renewable Energy Laboratory, Golden, Colorado 80401, United States;* orcid.org/0000-0002-4679-6556
Nathaniel Sunderlin − *National Renewable Energy Laboratory, Golden, Colorado 80401, United States*
Shriram Santhanagopalan − *National Renewable Energy Laboratory, Golden, Colorado 80401, United States;* orcid.org/0000-0003-4703-1341

Complete contact information is available at: https://pubs.acs.org/10.1021/acsaem.0c02260

Author Contributions

Conceptualization, K.F.; methodology, K.F., J.E.C., and N.S.; investigation, K.F.; formal analysis, K.F. and P.G.; writing, K.F. and P.G.; funding acquisition, S.S. All authors have given approval to the final version of the manuscript.

Funding

Funding for this work was provided by the U.S. Department of Energy (DOE) under Contract DE-AC36-08GO28308 through the ReCell Center for Advanced Battery Recycling.

Notes

The authors declare no competing financial interest.

■ ACKNOWLEDGMENTS

This work was authored by the Alliance for Sustainable Energy, LLC, the manager and operator of the National Renewable Energy Laboratory for the US DOE. This work was performed through the ReCell Center, which gratefully acknowledges support from the DOE, Office of Energy Efficiency and Renewable Energy, and the Vehicle Technologies Office. The views expressed in the article do not necessarily represent the views of the DOE or the US government. The US government and the publisher, by accepting the article for publication, acknowledge that the US government retains a nonexclusive, paid-up, irrevocable, worldwide license to publish or reproduce the published form of this work, or allow others to do so, for US government purposes.

■ REFERENCES

(1) *Global EV Outlook 2020*; International Energy Agency, 2020.
(2) Pillot, C. *The Rechargeable Battery Market and Main Trends 2018−2030*; BMW i Berlin E-Prix: Berlin, Germany, 2019.
(3) Marano, V.; Onori, S.; Guezennec, Y.; Rizzoni, G.; Madella, N. Lithium-ion batteries life estimation for plug-in hybrid electric vehicles. *Proceedings of the 2009 IEEE Vehicle Power and Propulsion Conference*; IEEE: Dearborn, MI, 2009; pp 536−543.
(4) Olsson, L.; Fallahi, S.; Schnurr, M.; Diener, D.; van Loon, P. Circular business models for extended EV battery life. *Batteries* **2018**, *4*, 57.
(5) Chen, M.; Ma, X.; Chen, B.; Arsenault, R.; Karlson, P.; Simon, N.; Wang, Y. Recycling End-of-Life Electric Vehicle Lithium-Ion Batteries. *Joule* **2019**, *3*, 2622−2646.
(6) Sloop, S. E.; Trevey, J. E.; Gaines, L.; Lerner, M. M.; Xu, W. Advances in Direct Recycling of Lithium-Ion Electrode Materials. *ECS Trans.* **2018**, *85*, 397−403.
(7) Sloop, S.; Crandon, L.; Allen, M.; Koetje, K.; Reed, L.; Gaines, L.; Sirisaksoontorn, W.; Lerner, M. A direct recycling case study from a lithium-ion battery recall. *Sustainable Mater. Technol.* **2020**, *25*, No. e00152.
(8) Amine, K.; Chen, C. H.; Liu, J.; Hammond, M.; Jansen, A.; Dees, D.; Bloom, I.; Vissers, D.; Henriksen, G. Factors responsible for impedance rise in high power lithium ion batteries. *J. Power Sources* **2001**, *97−98*, 684−687.
(9) Chen, C. H.; Liu, J.; Amine, K. Symmetric cell approach and impedance spectroscopy of high power lithium-ion batteries. *J. Power Sources* **2001**, *96*, 321−328.
(10) Andersson, A. M.; Abraham, D. P.; Haasch, R.; MacLaren, S.; Liu, J.; Amine, K. Surface Characterization of Electrodes from High Power Lithium-Ion Batteries. *J. Electrochem. Soc.* **2002**, *149*, A1358−A1369.
(11) Shikano, M.; Kobayashi, H.; Koike, S.; Sakaebe, H.; Ikenaga, E.; Kobayashi, K.; Tatsumi, K. Investigation of positive electrodes after cycle testing of high-power Li-ion battery cells II. *J. Power Sources* **2007**, *174*, 795−799.
(12) Rahman, M. K.; Saito, Y. Investigation of positive electrodes after cycle testing of high-power Li-ion battery cells. *J. Power Sources* **2007**, *174*, 889−894.
(13) Buchner, F.; Fingerle, M.; Kim, J.; Spath, T.; Hausbrand, R.; Behm, R. J. Interaction of Ultrathin Films of Ethylene Carbonate with Oxidized and Reduced Lithium Cobalt Oxide-A Model Study of the Cathode|Electrolyte Interface in Li-Ion Batteries. *Adv. Mater. Interfaces* **2019**, *6*, 1801650.
(14) Renfrew, S. E.; Kaufman, L. A.; McCloskey, B. D. Altering Surface Contaminants and Defects Influences the First-Cycle Outgassing and Irreversible Transformations of LiNi0.6Mn0.2-Co0.2O2. *ACS Appl. Mater. Interfaces* **2019**, *11*, 34913−34921.
(15) Waldmann, T.; Iturrondobeitia, A.; Kasper, M.; Ghanbari, N.; Aguesse, F.; Bekaert, E.; Daniel, L.; Genies, S.; Gordon, I. J.; Loble, M. W.; De Vito, E.; Wohlfahrt-Mehrens, M. Review-Post-Mortem Analysis of Aged Lithium-Ion Batteries: Disassembly Methodology and Physico-Chemical Analysis Techniques. *J. Electrochem. Soc.* **2016**, *163*, A2149−A2164.
(16) Williard, N.; Sood, B.; Osterman, M.; Pecht, M. Disassembly methodology for conducting failure analysis on lithium−ion batteries. *J. Mater. Sci.: Mater. Electron.* **2011**, *22*, 1616−1630.
(17) Somerville, L.; Bareno, J.; Jennings, P.; McGordon, A.; Lyness, C.; Bloom, I. The Effect of Pre-Analysis Washing on the Surface Film of Graphite Electrodes. *Electrochim. Acta* **2016**, *206*, 70−76.
(18) Fang, C.; Liu, Z.; Lau, J.; Elzouka, M.; Zhang, G.; Khomein, P.; Lubner, S.; Ross, P. N.; Liu, G. Gradient Polarity Solvent Wash for Separation and Analysis of Electrolyte Decomposition Products on Electrode Surfaces. *J. Electrochem. Soc.* **2020**, *167*, 020506.
(19) Dutkiewicz, M. Classification of organic solvents based on correlation between dielectric ? parameter and empirical solvent polarity parameter E N T. *J. Chem. Soc., Faraday Trans.* **1990**, *86*, 2237−2241.
(20) Fingerle, M.; Spath, T.; Schulz, N.; Hausbrand, R. Adsorption of ethylene carbonate on lithium cobalt oxide thin films: A synchrotron-based spectroscopic study of the surface chemistry. *Chem. Phys.* **2017**, *498−499*, 19−24.
(21) Murbach, M.; Gerwe, B.; Dawson-elli, N.; Tsui, L.-k. impedance.py: A Python package for electrochemical impedance analysis. *J. Open Source Software* **2020**, *5*, 2349.
(22) Schonleber, M.; Klotz, D.; Ivers-Tiffee, E. A Method for Improving the Robustness of linear Kramers-Kronig Validity Tests. *Electrochim. Acta* **2014**, *131*, 20−27.
(23) Osaka, T.; Mukoyama, D.; Nara, H. Review-Development of Diagnostic Process for Commercially Available Batteries, Especially Lithium Ion Battery, by Electrochemical Impedance Spectroscopy. *J. Electrochem. Soc.* **2015**, *162*, A2529−A2537.
(24) Dobelin, N.; Kleeberg, R. Profex: a graphical user interface for the Rietveld refinement program BGMN. *J. Appl. Crystallogr.* **2015**, *48*, 1573−1580.
(25) Horsthemke, F.; Friesen, A.; Monnighoff, X.; Stenzel, Y. P.; Grutzke, M.; Andersson, J. T.; Winter, M.; Nowak, S. Fast screening method to characterize lithium ion battery electrolytes by means of solid phase microextraction - gas chromatography - mass spectrometry. *RSC Adv.* **2017**, *7*, 46989−46998.
(26) Podias, A.; Pfrang, A.; Di Persio, F.; Kriston, A.; Bobba, S.; Mathieux, F.; Messagie, M.; Boon-Brett, L. Sustainability Assessment of Second Use Applications of Automotive Batteries: Ageing of Li-

Ion Battery Cells in Automotive and Grid-Scale Applications. *World Electr. Veh. J.* **2018**, *9*, 24.

(27) Wang, J.; Purewal, J.; Liu, P.; Hicks-Garner, J.; Soukazian, S.; Sherman, E.; Sorenson, A.; Vu, L.; Tataria, H.; Verbrugge, M. W. Degradation of lithium ion batteries employing graphite negatives and nickel-cobalt-manganese oxide + spinel manganese oxide positives: Part 1, aging mechanisms and life estimation. *J. Power Sources* **2014**, *269*, 937−948.

(28) Fink, K.; Santhanagopalan, S.; Hartig, J.; Cao, L. Characterization of Aged Li-Ion Battery Components for Direct Recycling Process Design. *J. Electrochem. Soc.* **2019**, *166*, A3775−A3783.

(29) Assat, G.; Foix, D.; Delacourt, C.; Iadecola, A.; Dedryvere, R.; Tarascon, J.-M. Fundamental interplay between anionic/cationic redox governing the kinetics and thermodynamics of lithium-rich cathodes. *Nat. Commun.* **2017**, *8*, 2219.

(30) Assat, G.; Iadecola, A.; Foix, D.; Dedryvere, R.; Tarascon, J.-M. Direct Quantification of Anionic Redox over Long Cycling of Li-Rich NMC via Hard X-ray Photoemission Spectroscopy. *ACS Energy Lett.* **2018**, *3*, 2721−2728.

(31) Gallagher, K. G.; Croy, J. R.; Balasubramanian, M.; Bettge, M.; Abraham, D. P.; Burrell, A. K.; Thackeray, M. M. Correlating hysteresis and voltage fade in lithium- and manganese-rich layered transition-metal oxide electrodes. *Electrochem. Commun.* **2013**, *33*, 96−98.

(32) Zhang, L.; Xu, Z.; He, Z. Electrochemical Relithiation for Direct Regeneration of LiCoO2 Materials from Spent Lithium-Ion Battery Electrodes. *ACS Sustainable Chem. Eng.* **2020**, *8*, 11596−11605.

(33) Assat, G.; Tarascon, J.-M. Fundamental understanding and practical challenges of anionic redox activity in Li-ion batteries. *Nat. Energy* **2018**, *3*, 373−386.

(34) Zheng, X.; Li, X.; Wang, Z.; Guo, H.; Huang, Z.; Yan, G.; Wang, D. Investigation and improvement on the electrochemical performance and storage characteristics of LiNiO2-based materials for lithium ion battery. *Electrochim. Acta* **2016**, *191*, 832−840.

(35) Sun, Y.; Li, N.; Xing, X.; Zhang, X.; Zhang, Z.; Wang, G.; Cheng, J.; Hao, Z. Catalytic oxidation performances of typical oxygenated volatile organic compounds (acetone and acetaldehyde) over MAlO (M = Mn, Co, Ni, Fe) hydrotalcite-derived oxides. *Catal. Today* **2019**, *327*, 389−397.

(36) Golodets, G. I.; Pavlenko, N. V.; Gun'ko, V. M.; Tel'biz, G. M. Investigation of the reaction of acetone and acetonitrile molecules with the surfaces of metallic catalysts by IR-spectroscopic and quantum chemical methods. *Theor. Exp. Chem.* **1989**, *24*, 526−533.

(37) Bielanski, A.; Haber, J. Oxygen in Catalysis on Transition Metal Oxides. *Catal. Rev.: Sci. Eng.* **1979**, *19*, 1.

(38) Pritzl, D.; Landesfeind, J.; Solchenbach, S.; Gasteiger, H. A. An Analysis Protocol for Three-Electrode Li-Ion Battery Impedance Spectra: Part II. Analysis of a Graphite Anode Cycled vs. LNMO. *J. Electrochem. Soc.* **2018**, *165*, A2145−A2153.

(39) Gantenbein, S.; Weiss, M.; Ivers-Tiffee, E. Impedance based time-domain modeling of lithium-ion batteries: Part I. *J. Power Sources* **2018**, *379*, 317−327.

(40) Mohanty, D.; Sefat, A. S.; Li, J.; Meisner, R. A.; Rondinone, A. J.; Payzant, E. A.; Abraham, D. P.; Wood, D. L., III; Daniel, C. Correlating cation ordering and voltage fade in a lithium-manganese-rich lithium-ion battery cathode oxide: a joint magnetic susceptibility and TEM study. *Phys. Chem. Chem. Phys.* **2013**, *15*, 19496−19509.

(41) Mohanty, D.; Kalnaus, S.; Meisner, R. A.; Rhodes, K. J.; Li, J.; Payzant, E. A.; Wood, D. L., III; Daniel, C. Structural transformation of a lithium-rich Li1.2Co0.1Mn0.55Ni0.15O2 cathode during high voltage cycling resolved by in situ X-ray diffraction. *J. Power Sources* **2013**, *229*, 239−248.

(42) Shi, Y.; Chen, G.; Liu, F.; Yue, X.; Chen, Z. Resolving the compositional and structural defects of degraded LiNixCoyMnzO2 particles to directly regenerate high-performance lithium-ion battery cathodes. *ACS Energy Lett.* **2018**, *3*, 1683−1692.

(43) Shinova, E.; Stoyanova, R.; Zhecheva, E.; Ortiz, G.; Lavela, P.; Tirado, J. Cationic distribution and electrochemical performance of LiCo1/3Ni1/3Mn1/3O2 electrodes for lithium-ion batteries. *Solid State Ionics* **2008**, *179*, 2198−2208.

(44) Hausbrand, R.; Cherkashinin, G.; Ehrenberg, H.; Groting, M.; Albe, K.; Hess, C.; Jaegermann, W. Fundamental degradation mechanisms of layered oxide Li-ion battery cathode materials: Methodology, insights and novel approaches. *Mater. Sci. Eng. B* **2015**, *192*, 3−25.

(45) Zheng, J.; Yan, P.; Zhang, J.; Engelhard, M. H.; Zhu, Z.; Polzin, B. J.; Trask, S.; Xiao, J.; Wang, C.; Zhang, J. Suppressed oxygen extraction and degradation of LiNi x Mn y Co z O2 cathodes at high charge cut-off voltages. *Nano Res.* **2017**, *10*, 4221−4231.

(46) Jung, S.-K.; Gwon, H.; Hong, J.; Park, K.-Y.; Seo, D.-H.; Kim, H.; Hyun, J.; Yang, W.; Kang, K. Understanding the Degradation Mechanisms of LiNi0.5Co0.2Mn0.3O2 Cathode Material in Lithium Ion Batteries. *Adv. Energy Mater.* **2018**, *4*, 1300787.

(47) Hu, E.; Wang, X.; Yu, X.; Yang, X.-Q. Probing the Complexities of Structural Changes in Layered Oxide Cathode Materials for Li-Ion Batteries during Fast Charge-Discharge Cycling and Heating. *Acc. Chem. Res.* **2018**, *51*, 290−298.

(48) Mohanty, D.; Gabrisch, H. Microstructural investigation of LixNi1/3Mn1/3Co1/3O2 ($x \leq 1$) and its aged products via magnetic and diffraction study. *J. Power Sources* **2012**, *220*, 405−412.

(49) Grutzke, M.; Kraft, V.; Weber, W.; Wendt, C.; Friesen, A.; Klamor, S.; Winter, M.; Nowak, S. Supercritical carbon dioxide extraction of lithium-ion battery electrolytes. *J. Supercrit. Fluids* **2014**, *94*, 216−222.

(50) Terborg, L.; Weber, S.; Passerini, S.; Winter, M.; Karst, U.; Nowak, S. Development of Gas Chromatographic Methods for the Analyses of Organic Carbonate-Based Electrolytes. *J. Power Sources* **2014**, *245*, 836−840.

(51) Gachot, G.; Grugeon, S.; Jimenez-Gordon, I.; Eshetu, G. G.; Boyanov, S.; Lecocq, A.; Marlair, G.; Pilard, S.; Laruelle, S. Gas Chromatography/Fourier Transform Infrared/Mass Spectrometry Coupling: A Tool for Li-Ion Battery Safety Field Investigation. *Anal. Methods* **2014**, *6*, 6120−6124.

(52) Nedjalkov, A.; Meyer, J.; Kohring, M.; Doering, A.; Angelmahr, M.; Dahle, S.; Sander, A.; Fischer, A.; Schade, W. Toxic Gas Emissions from Damaged Lithium Ion Batteries-Analysis and Safety Enhancement Solution. *Batteries* **2016**, *2*, 5.

(53) Spath, T.; Becker, D.; Schulz, N.; Hausbrand, R.; Jaegermann, W. Understanding the SEI Formation at Pristine Li-Ion Cathodes: Chemisorption and Reaction of DEC on LiCoO2 Surfaces Studied by a Combined SXPS/HREELS Approach. *Adv. Mater. Interfaces* **2017**, *4*, 1700567.

(54) Wandt, J.; Freiberg, A. T. S.; Ogrodnik, A.; Gasteiger, H. A. Singlet oxygen evolution from layered transition metal oxide cathode materials and its implications for lithium-ion batteries. *Mater. Today* **2018**, *21*, 825−833.

(55) Metzger, M.; Strehle, B.; Solchenbach, S.; Gasteiger, H. A. Hydrolysis of Ethylene Carbonate with Water and Hydroxide under Battery Operating Conditions. *J. Electrochem. Soc.* **2016**, *163*, A1219−A1225.

(56) Yang, Y.-L.; Ramaswamy, S. G.; Jakoby, W. B. Enzymatic Hydrolysis of Organic Cyclic Carbonates. *J. Biol. Chem.* **1998**, *273*, 7814−7817.

(57) Lee, J.-C.; Litt, M. H. Ring-Opening Polymerization of Ethylene Carbonate and Depolymerization of Poly(ethylene oxide-co-ethylene carbonate). *Macromolecules* **2000**, *33*, 1618−1627.

(58) Gan, H.; Takeuchi, E. S. Nitrate Additives for Nonaqueous Electrolyte Rechargeable Cells. U.S. Patent 6,136,477 A, 2000.

(59) Abe, K.; Takaya, T.; Yoshitake, H.; Ushigoe, Y.; Yoshio, M.; Wang, H. Functional Electrolyte: Additives for Improving the Cyclability of Cathode Materials. *Electrochem. Solid-State Lett.* **2004**, *7*, A462−A465.

https://dx.doi.org/10.1021/acsaem.0c02260
ACS Appl. Energy Mater. XXXX, XXX, XXX−XXX

(60) Mao, H.; Von Sacken, U. Aromatic Monomer Gassing Agents for Protecting Non-Aqueous Lithium Batteries against Overcharge. Canada Patent CA2163187A1, 1997.
(61) Lee, H.; Lee, J. H.; Ahn, S.; Kim, H.-J.; Cho, J.-J. Co-Use of Cyclohexyl Benzene and Biphenyl for Overcharge Protection of Lithium-Ion Batteries. *Electrochem. Solid-State Lett.* **2006**, *9*, A307−A310.
(62) Xiao, L.; Ai, X.; Cao, Y.; Yang, H. Electrochemical Behavior of Biphenyl as Polymerizable Additive for Overcharge Protection of Lithium Ion Batteries. *Electrochim. Acta* **2004**, *49*, 4189−4196.
(63) Korepp, C.; Kern, W.; Lanzer, E. A.; Raimann, P. R.; Besenhard, J. O.; Yang, M.; Moller, K.-C.; Shieh, D.-T.; Winter, M. 4-Bromobenzyl isocyanate versus benzyl isocyanate-New film-forming electrolyte additives and overcharge protection additives for lithium ion batteries. *J. Power Sources* **2007**, *174*, 637−642.
(64) Naji, A.; Ghanbaja, J.; Willmann, P.; Billaud, D. New Halogenated Additives to Propylene Carbonate-Based Electrolytes for Lithium-Ion Batteries. *Electrochim. Acta* **2000**, *45*, 1893−1899.
(65) Tsujioka, S.; Takase, H.; Takahashi, M.; Sugimoto, H.; Koide, M. Electrolyte for Electrochemical Device. U.S. Patent 0,081,496 A1, 2002.
(66) Wang, X.; Naito, H.; Sone, Y.; Segami, G.; Kuwajima, S. New Additives to Improve the First-Cycle Charge-Discharge Performance of a Graphite Anode for Lithium-Ion Cells. *J. Electrochem. Soc.* **2005**, *152*, A1996−A2001.
(67) Zhang, S. S. A Review on Electrolyte Additives for Lithium-Ion Batteries. *J. Power Sources* **2006**, *162*, 1379−1394.
(68) Saidi, M. Y.; Gao, F.; Barker, J.; Scordilis-Kelley, C. Additive to Stabilize Electrochemical Cell. U.S. Patent 5,846,673 A, 1998.
(69) Zhang, Z.; Xu, X.; Zuo, X.-X.; Li, W.-S. Stabilizing Effect of Amine on Small Molecules in Electrolyte of Lithium Batteries. *Acta Phys.-Chim. Sin.* **2007**, *23*, 526.
(70) Shukla, K.; Srivastava, V. C. Efficient Synthesis of Diethyl Carbonate from Propylene Carbonate and Ethanol Using Mg-La Catalysts: Characterization, Parametric, and Thermodynamic Analysis. *Ind. Eng. Chem. Res.* **2018**, *57*, 12726−12735.

https://dx.doi.org/10.1021/acsaem.0c02260
ACS Appl. Energy Mater. XXXX, XXX, XXX−XXX